Synaptotagmin 7 docks synaptic vesicles for Doc2α-triggered asynchronous neurotransmitter release

Zhenyong Wu[1,2*], Grant F. Kusick[3,4*], Sumana Raychaudhuri[3], Kie Itoh[3], Edwin R. Chapman[1,2] & Shigeki Watanabe[3,5]

[1]Department of Neuroscience, University of Wisconsin-Madison, Madison, USA
[2]Howard Hughes Medical Institute, Madison, USA
[3]Department of Cell Biology, Johns Hopkins University, School of Medicine, Baltimore, MD, USA.
[4]Biochemistry, Cellular and Molecular Biology Graduate Program, Johns Hopkins University, School of Medicine, Baltimore, MD, USA.
[5]Solomon H. Snyder Department of Neuroscience, Johns Hopkins University, School of Medicine, Baltimore, MD, USA
[*]These authors contributed equally to the manuscript

Correspondence:
Shigeki Watanabe (shigeki.watanabe@jhmi.edu)
Edwin R. Chapman (chapman@wisc.edu)

Keywords
Synaptic vesicle, exocytosis, neurotransmitter release, synaptotagmin 7, Doc2, asynchronous release, short-term plasticity, facilitation, synaptic vesicle docking, zap-and-freeze, iGluSnFR

Abstract
The molecular basis of asynchronous neurotransmitter release remains enigmatic despite decades of intense study. Synaptotagmin (syt) 7 and Doc2 have both been proposed as Ca^{2+} sensors that trigger this mode of exocytosis, but conflicting findings have led to controversy. Here, we demonstrate that at excitatory mouse hippocampal synapses, Doc2α is the major Ca^{2+} sensor for asynchronous release, while syt7 supports this process through activity-dependent docking of synaptic vesicles. In synapses lacking Doc2α, asynchronous release after single action potentials is strongly reduced, while deleting syt7 has no effect. However, in the absence of syt7, docked vesicles cannot recover on millisecond timescales. Consequently, both synchronous and asynchronous release depress from the second pulse on during repetitive activity. By contrast, synapses lacking Doc2α have normal activity-dependent docking, but continue to exhibit decreased asynchronous release after multiple stimuli. Moreover, disruption of both Ca^{2+} sensors is non-additive. These findings result in a new model whereby syt7 drives activity-dependent docking, thus 'feeding' synaptic vesicles to Doc2 for asynchronous release during on-going transmission.

Introduction
Ca^{2+}-triggered neurotransmitter release involves at least two kinetically distinct components: one synchronous, which sets in after tens of microseconds (Sabatini and Regehr, 1996) of a stimulus and completes within several milliseconds, and another asynchronous, which sets in more slowly and can persist for tens or hundreds of milliseconds (Goda and Stevens, 1994; Kaeser and Regehr, 2014). The molecular basis of synchronous release has been characterized in depth, and there is broad agreement that the underlying Ca^{2+} sensors are two members of the synaptotagmin (syt) family of proteins, isoforms 1 and 2 (Stevens and Sullivan, 2003). The Ca^{2+} sensors that regulate asynchronous release (AR), however, remain a subject of controversy.

AR is thought to play a critical role in information processing and circuit function (Iremonger and Bains, 2007; Kaeser and Regehr, 2014; Manseau et al., 2010) and has been implicated in epileptiform activity in rats and humans (Jiang et al., 2012). However, it is impossible to test how slow transmission impacts neural networks without knowing proteins that are specifically required for AR. The unambiguous identification of the underlying Ca^{2+} sensors would enable systematic perturbation of AR, thus enabling experiments on its importance for information processing.

Two classes of proteins have been proposed as Ca^{2+} sensors for AR in vertebrates: Doc2 and syt7. Two isoforms of Doc2, α and β function as Ca^{2+} sensors; α mediates AR in hippocampal neurons, and loss of AR in α KO neurons can be rescued by β (Yao et al., 2011). Both Doc2 and syt7 exhibit the slow Ca^{2+}-regulated membrane-binding kinetics and high affinity required for AR (Hui et al., 2005; Xue et al., 2015; Yao et al., 2011). In cultured hippocampal neurons, Doc2α drives significant levels of AR

both after single action potentials and during trains (Gaffaney et al., 2014; Xue et al., 2015, 2018; Yao et al., 2011). However, no significant changes in AR were observed in Purkinje cell to deep cerebellar nuclei synapses (Khan and Regehr, 2020) and in autaptic cultured hippocampal neurons lacking Doc2 (Groffen et al., 2010). These varying results have left the importance of Doc2 for AR in doubt.

Syt7 has received more attention (Huson and Regehr, 2020), but its exact role in AR is still hotly debated. Syt7 is important for AR at the zebrafish neuromuscular junction (Wen et al., 2010). However, conflicting evidence has accumulated for mammalian central synapses. In syt7 knockout (KO) mouse cortical neurons, no synaptic phenotypes were initially observed (Maximov et al., 2008). However, later studies, inspired by the work in zebrafish, found defects in AR – in cultured hippocampal neurons (Bacaj et al., 2013), inhibitory synapses formed between basket cells and Purkinje neurons as well as granule cell synapses in the cerebellum (Chen et al., 2017; Turecek and Regehr, 2018), and in excitatory synapses between pyramidal cells and Martinotti neurons in the neocortex (Deng et al., 2020). However, unlike Doc2α, the role of syt7 in AR is usually only apparent when more than one stimulus is applied. Among these studies, deleting syt7 decreased AR—after a single action potential—only in granule cell synapses (Turecek and Regehr, 2018) and in syt1 KO cultured hippocampal neurons (Bacaj et al., 2013). In inhibitory synapses of the inferior olive, where release after single action potentials is often highly asynchronous, deleting syt7 actually makes release even slower (Turecek and Regehr, 2019). Thus, the importance of these two sensors, syt7 and Doc2α, in AR may depend, at least in part, on the frequency of stimulation, the number of stimuli applied, and the synapse under study.

To reconcile the function of these proteins in AR, we performed glutamate sensor imaging, electrophysiology, and zap-and-freeze electron microscopy experiments in mouse hippocampal neurons. AR after single action potentials was strongly reduced in Doc2α KOs, but not in syt7 KOs, suggesting that Doc2α mediates AR. In contrast, AR during train stimulation was reduced to a similar extent in both syt7 and Doc2α KO neurons. Ultrastructural analysis revealed that, in syt7 KO neurons, docked vesicles fail to recover on millisecond timescales (Kusick et al., 2020). Consequently, both synchronous and asynchronous release quickly and profoundly depress during train stimulation. By contrast, in Doc2α KO neurons this syt7-dependent ultrafast recruitment of vesicles was unaffected. Thus, with AR largely absent, more newly recruited vesicles are available for synchronous release, leading to slower depression in Doc2α KO neurons. AR in Doc2α /syt7 DKO neurons was similar to Doc2α KO, consistent with these two proteins acting in sequence, rather than as parallel sensors for release. These data indicate that syt7 supplies docked vesicles for synchronous release and Doc2α-mediated AR during repetitive stimulation.

Results

Doc2, but not syt7, mediates asynchronous release after single action potentials

First, to directly monitor glutamate release, we transduced an optical glutamate reporter (iGluSnFR) into cultured mouse hippocampal neurons (Marvin et al., 2013, 2018; Figures 1A,B, and S1). This approach bypasses postsynaptic factors that influence the time course of transmission as monitored using traditional patch-clamp recordings, and allows individual AR events to be measured directly (Vevea et al., 2021). We applied a single stimulus and monitored the timing of glutamate release at the single-bouton level (Figure 1B) from Doc2α knockout (KO, *Doc2α*$^{em1Smoc/em1Smoc}$) and syt7 KO (*Syt7*$^{tm1Nan/tm1Nan}$) neurons and their respective wild-type littermates (WT – *Doc2α*$^{+/+}$ or *Syt7*$^{+/+}$). The peak of fluorescence was used as the timing of each release event and plotted as a histogram with each bin being 10 ms (Figure 1B). Peaks detected after 10 ms were defined as the asynchronous component of release (Vevea and Chapman, 2020).

In the WT, 64% of release occurred within 10 ms of the action potential (synchronous release: n = 1000 events); the rest of the events (36%) were defined as asynchronous (Figure 1B; n = 1000 events). This interpretation is further supported by the data from WT neurons treated with EGTA-AM, which selectively reduces AR by chelating residual Ca^{2+} (Chen and Regehr, 1999). This treatment greatly reduced AR (Figure 1B, 88% in the first bin, 11 % in the second, and 1% in the third), consistent with previous work using this approach (Vevea and Chapman, 2020). Syt7 KO neurons had no apparent phenotype (Figure 1B-E; 66% synchronous and 34% asynchronous, p = 0.39). The 2% reduction in AR in the KO did not reach statistical significance here, but we note that this trend is consistent with earlier measurements using iGluSnFR (Figure 1B, C; p = 0.39, against WT) (Vevea et al., 2021). By contrast, the asynchronous component was markedly reduced in Doc2α KO neurons (Figure 1B-E, C; 84% synchronous and 16% asynchronous). While the amount of AR in Doc2α KO was slightly greater than in EGTA-treated WT neurons, this difference was not statistically significant (p = 0.12). These findings indicate that Doc2α is required for the majority of AR. The peak average fluorescence intensity in both mutants was similar to WT (Figure 1D), demonstrating that synchronous release is not affected in these mutants (Vevea et al., 2021; Yao et al., 2011).

We next turned to acute hippocampal slices to assay Doc2α and syt7 function in a native circuit. We applied a single stimulus to Schaffer collaterals and measured evoked excitatory postsynaptic currents (EPSCs) from CA1 neurons by whole-cell patch clamp (Figures 2A, and S3A,B). As with iGluSnFR imaging in cultured neurons (Figure 1), syt7 KOs showed no phenotype – the amplitude and kinetics of EPSCs were nearly identical to those of WT (Figure 2B-D). By contrast, in Doc2α KO, the EPSC amplitude was unchanged, but the total charge transfer was reduced by 35% (Figure 2B-D). Cumulative charge transfer data were fitted with double exponential functions, reflecting

two kinetic components of release (Figure 2C; Goda and Stevens, 1994). The fast component, representing synchronous release, was similar across all three genotypes. However, the slow, asynchronous component was reduced by 61% in Doc2α KO neurons ($p<0.0001$); no changes in the asynchronous component were observed in syt 7 KOs (Figure 2D). EGTA-AM treatment of WT slices reduced the slow component slightly more severely than Doc2α KO (Figure 2B-D; $p = 0.03$ against Doc2α KO). Finally, the time constants for both components of evoked EPSCs were similar across all genotypes (Figure 2D). Together, these data suggest that AR after single action potentials is driven by Doc2α, but not syt7, in excitatory mouse hippocampal synapses.

Both Doc2α and syt7 are essential for asynchronous release after repeated action potentials

We then addressed the roles of Doc2α and syt7 in AR during sustained stimulation. We stimulated cultured hippocampal neurons 50 times at 10 and 20 Hz and measured iGluSnFR responses (Figure 3A). To resolve the response from each pulse during the train, we used the faster, low-affinity version of iGluSnFR (S72A; Marvin et al., 2018; Vevea et al., 2021). At 20 Hz, WT neurons exhibited facilitation of synchronous release in response to the second pulse, and thereafter depressed as the train went on, eventually reaching a steady state (Figure 3B, D). In contrast to synchronous release, the amount of AR remained mostly constant through repeated stimuli in WT neurons, only gradually decreasing late in the train at 10 Hz but not at 20 Hz (Figure 3C). The paired-pulse ratio of Doc2α KO neurons was similar to WT. However, in KO neurons, slower synaptic depression occurred from the third action potential onward, eventually reaching the same steady-state depression as WT, later in the train. This is consistent with the idea that attenuation of AR spares some vesicles for ongoing synchronous release (Otsu et al., 2004; Yao et al., 2011).

In contrast, syt7 KO neurons displayed depression instead of facilitation of synchronous release after the second pulse, as well as faster and more severe synaptic depression as the train progressed (Figure 3D). This result is in line with a large body of work showing that syt7 is essential for both facilitation and resistance to depression (Chen et al., 2017; Jackman et al., 2016; Liu et al., 2014; Vevea et al., 2021). As in single-stimulus measurements (Figure 1), AR was decreased in Doc2α KOs, but not syt7 KOs, after the first pulse of the stimulus train. However, after the second action potential both Doc2α KOs *and* syt7 KOs showed a similar reduction in AR. This effect continued through the train, such that the cumulative AR was reduced by 40% in syt7 KOs and 33% in Doc2α KO neurons (Figure 3A-C; see also (Vevea et al., 2021)). We also analyzed the spatial distribution of the iGluSnFR signals from 923 boutons and did not observe spatial segregation of AR during the first two responses (see Figure S2 for further analysis and details). Together, these data suggest that both Doc2α and syt7 contribute to AR from the second pulse onward during the train.

Next, we examined AR during train stimulation in hippocampal slices (Figures 4A and S3A,B); these results confirmed our findings using cultured neurons. Peak amplitudes (synchronous release) depressed more slowly in Doc2α KOs, while syt7 KOs exhibited depression instead of facilitation after the second action potential, as well as faster and more profound synaptic depression (Figure 4B). Surprisingly, loss of syt7 caused more severe defects in short-term plasticity than EGTA-AM. While EGTA-AM blocked facilitation after the second action potential, from the third action potential onward amplitudes were similar to untreated WT neurons. Both syt7 and Doc2α KO neurons exhibited a 60% reduction in the slow charge transfer component from the second action potential onward, consistent with decreased AR. These phenotypes were only marginally less severe than in the EGTA-AM treatment condition (69%) (Figures 4C and S3D). Together, these data further demonstrate that while only Doc2α mediates AR after single action potentials, both Doc2α and syt7 are critical during sustained activity.

Doc2α mediates asynchronous fusion, while syt7 docks vesicles

Why is Doc2α essential for AR after single and multiple stimuli, while syt7 is only required starting with a second action potential? And why is short-term plasticity so catastrophically disrupted in syt7 KOs? Recent studies have proposed that synaptic vesicles rapidly transition from undocked to docked states during activity, and that this could, in principle, provide a common basis for AR synaptic facilitation, and resistance to synaptic depression (Chang et al., 2018; Kusick et al., 2022; Miki et al., 2016, 2018; Neher and Brose, 2018; Silva et al., 2021). In this model, after Ca^{2+} influx, initially undocked and release-incompetent vesicles can dock and fuse ('two-step' release; Blanchard et al., 2020; Miki et al., 2018), resulting in AR, or dock and then fuse after another action potential, leading to facilitation and resistance to depression (Miki et al., 2016; Neher and Brose, 2018). Consistent with this notion, we previously found that vesicles can dock within 15 ms of an action potential to replenish vacated release sites (Kusick et al., 2020). Importantly, like AR and facilitation, this 'transient docking' is blocked by EGTA-AM. Thus, our imaging and electrophysiology findings could be explained by these two Ca^{2+} sensors playing distinct roles in docking and fusion, with Doc2α triggering AR, while syt7 mediates transient docking.

To test this hypothesis, we performed zap-and-freeze electron microscopy experiments (Kusick et al., 2020). This approach allows us to measure synchronous and asynchronous vesicle fusion, as well as depletion and replenishment of docked vesicles, in the same experiment. Vesicles that appear to be in contact with the plasma membrane are considered docked. Unstimulated syt7 KO and Doc2α KO synapses appeared qualitatively normal (see Figures 5A-D, 6A-D, and S4 for example micrographs). Knocking out either protein did not affect the number of docked vesicles (Figure 6D-E) nor the number and distribution of synaptic vesicles within 100 nm of the

plasma membrane at the active zone (Figure S5D). Therefore, the physiological defects in syt7 and Doc2α synapses cannot be accounted for by any ultrastructural phenotypes at rest.

We then measured exocytosis by applying a single stimulus (1 ms, 1.2 mM external Ca^{2+}, 37 ºC) and freezing the neurons at 5, 11, and 14 ms after the action potential. These time points capture synchronous fusion, asynchronous fusion, and transient docking, respectively (Kusick et al., 2020; Li et al., 2021). Consistent with our previous findings (Kusick et al., 2020; Li et al., 2021), in WT controls exocytic pits peaked at 5 ms after an action potential, declined to less than half of this peak at 11 ms, then further declined to baseline by 14 ms (Figure 5E,F; pits in the active zone per synaptic profile: syt7 WT: no stim: 0.03 pits; 5 ms; 0.22 pits; 11 ms: 0.13 pits; 14 ms: 0.04 pits; Doc2α WT: no stim: 0.021 pits; 5 ms: 0.35 pits; 11 ms: 0.08 pits; 14 ms: 0.04 pits. See Figure S5A for active zone sizes from each condition and Figure S5B for pit data normalized to the size of active zones). In syt7 KOs, this sequence was unchanged: the number of pits at each time point in the KO was not different from the corresponding WT control (pits per synaptic profile: syt7 KO: no stim: 0.04 pits; 5 ms: 0.28 pits; 11 ms: 0.14 pits; 14 ms: 0.06 pits; $P > 0.9$ for each compared to the corresponding syt7 WT time point). By contrast, in Doc2α KO synapses, the number of pits at 5 ms was unchanged, but pits at 11 ms were almost completely abolished (pits per synaptic profile: Doc2α KO: no stim: 0.02 pits; 5 ms: 0.32 pits; 11 ms: 0.03 pits; 14 ms: 0.01 pits; $P = 0.04$ between WT and KO 11 ms, $P = 0.02$ between WT no stim and 11 ms, $P > 0.9$ between KO no stim and 11 ms). This phenotype mirrors the effect of EGTA-AM we previously reported (Kusick et al., 2020), consistent with Doc2α being essential for residual Ca^{2+}-dependent AR. In sum, we obtained the same result from three different techniques (iGluSnFR imaging, patch-clamp electrophysiology, and zap-and-freeze electron microscopy): after a single action potential, Doc2α accounts for 54-67% of AR at hippocampal excitatory synapses, whereas deleting syt7 has no effect.

Is syt7 required for activity-dependent transient docking of synaptic vesicles? To test this possibility, we quantified all vesicles within 100 nm of the plasma membrane at the active zone. The distribution of undocked vesicles did not change in any of the genotypes, nor did it change after stimulation (Figure S5D). WT controls showed rapid depletion and replenishment of docked vesicles after an action potential, as previously reported (Kusick et al., 2020) (Figure 6E,F.). At 5 and 11 ms, there were ~40% fewer docked vesicles than in the no-stim controls, then at 14 ms docked vesicles returned to baseline (Figure 6E,F; docked vesicles per synaptic profile: syt7 WT: no stim: 2.19; 5 ms; 1.52; 11 ms: 1.36; 14 ms: 1.93; Doc2α WT: no stim: 1.90; 5 ms: 0.91; 11 ms: 1.00; 14 ms: 1.62. See Figure S5A for active zone sizes from each condition and Figure S5C for docked vesicle data normalized to the size of active zones). In syt7 KO, consistent with our previous data (Vevea et al., 2021), there were ~25% fewer docked vesicles than in WT controls at 5 ms and 11 ms. At 14 ms, docked vesicles completely failed to

recover in syt7 KO, remaining at less than half of the no-stim control (docked vesicles per synaptic profile: syt7 KO: no stim: 2.12; 5 ms: 1.07; 11 ms: 1.07; 14 ms: 1.09; $P < 0.0001$ between WT and KO at 14 ms, $P = 0.001$ at 5 ms between WT and KO, $P = 0.16$ at 5 ms between WT and KO). These data indicate that syt7 is absolutely required for transient docking of synaptic vesicles.

In Doc2α KO neurons, by contrast, we observed normal docked vesicle depletion and faster recovery (Figure 6F). The number of docked vesicles was 40% greater in the KO than in the WT at 11 ms, about halfway towards full recovery to baseline (docked vesicles per synaptic profile: Doc2α KO: no stim: 1.85; 5 ms; 1.11; 11 ms: 1.40; 14 ms: 1.63; $P < 0.0001$ between WT and KO at 11 ms, $P < 0.0001$ between 11 ms and no stim in the KO). This is consistent with the slower train depression in Doc2α KOs (Figures 3, 4, and S3C) and may result from vesicles being spared by the lack of AR. We conclude that transient docking completely fails in the absence of syt7, while Doc2α is dispensable for docked vesicle recovery. Taken together with our data on exocytosis, these results suggest that syt7 supports synchronous and AR after multiple stimuli by triggering transient docking, while Doc2 is the Ca^{2+} sensor for asynchronous fusion itself.

In a final series of experiments, we tested the sequential action of syt7 and Doc2α by conducting an epistasis experiment using double knockout (DKO) mice. If syt7 and Doc2α act as parallel Ca^{2+} sensors triggering AR directly, rather than in sequence through transient docking (syt7) and fusion (Doc2α), the DKO would be expected to eliminate or reduce the remaining AR from either of the single knockouts. For these experiments we conducted hippocampal slice electrophysiology. We first applied single action potentials and observed that loss of both proteins was not additive: the reduction in AR was identical in Doc2α neurons as compared to Doc2α/syt7 DKOs. EGTA-AM produced a slightly stronger effect than either Doc2α KO or DKO of both sensors (Figure 7A,B), indicating that the remaining AR in Doc2α KO neurons is not mediated by syt7. We then applied train stimulation (Figure 7C) and quantified the cumulative asynchronous charge transfer (Figure 7D). Again, no differences were observed between the Doc2α KO and the Doc2α/syt7 DKO condition (the inset in Figure 7D shows the first three responses on an expanded scale). In DKOs, short-term plasticity of synchronous release early in the train was similar to EGTA-treated neurons, with abolished paired-pulse facilitation but not the enhanced depression seen in syt7 KOs. This is consistent with the idea that disrupting asynchronous release, but not transient docking, produces the slower depression in Doc2α KOs, while disrupting transient docking, but not asynchronous release, causes the faster depression in syt7 KOs. Disrupting both, with EGTA or DKO, balances out to a similar rate of depression as the WT. However, late in the train amplitudes decayed to the same lower level as syt7 KOs, indicating a specific role for syt7 in limiting steady-state depression (Figure

S6). Together, these findings strongly support a sequential model for the action of syt7 and Doc2α (illustrated in Figure S7, as detailed below).

Discussion

Resolving the asynchronous release Ca^{2+} sensor controversy

Both Doc2α (Yao et al., 2011) and syt7 (Wen et al., 2010) have been implicated in AR, but conflicting results over the years led to an unresolved debate - which sensor mediates AR? Several factors may have contributed to these inconsistent results, including stimulation frequency, the type of synapse under study, and method used to measure release. To minimize the effects from these different factors, we conducted a side-by-side comparison of Doc2α and syt7 KO neurons, under identical conditions, using direct optical measurements of glutamate release, patch clamp electrophysiology, and ultrastructural characterization of millisecond-by-millisecond vesicle dynamics from cultured mouse hippocampal neurons. These experiments show that Doc2α drives significant levels of AR after a single action potential. In sharp contrast, syt7 has a negligible effect on this mode of release in response to a single action potential. Remarkably, during a stimulus train, both Doc2α and syt7 are equally important for AR. These results resolve some of the inconsistencies in the literature. First, Doc2α is a Ca^{2+} sensor for AR both after a single stimulus, and also during the train in both cultured hippocampal neurons and Schaffer collaterals. Second, syt7 contributes to AR, but its role is only apparent from the second action potential onward. Thus, at least in mouse hippocampal synapses, these sensors both contribute to AR. However, it is still likely that which sensor(s) are required depends on synapse type, and we reiterate that Doc2β played no apparent role in transmission at Purkinje cell to deep cerebellar nuclei synapses (Khan and Regehr, 2020). Thus, further work should explore the diversity of synaptic Ca^{2+} sensors and how they contribute to heterogeneity in synaptic transmission throughout the brain.

Sequential action of syt7 and Doc2 in asynchronous release

How syt7 contributes to three separate phenomena, paired-pulse facilitation, AR, and resistance to synaptic depression, has emerged as a major question in the field (Huson and Regehr, 2020; Jackman and Regehr, 2017; Liu et al., 2014; Vevea et al., 2021). Our data suggest that syt7 drives activity-dependent transient docking to support all three processes; in the case of paired-pulse facilitation it feeds docked vesicles to syt1 to enhance release in response to the second stimulus; it likely functions in the same manner to reduce synaptic depression during train stimulation. In the case of AR, it feeds vesicles to Doc2α, which then directly triggers this slow mode of transmission, again after the first stimulus. This is consistent with the recent proposal that activity-

dependent docking underlies both short-term plasticity and AR (Miki et al., 2016, 2018; Neher and Brose, 2018; Silva et al., 2021).

Three pieces of data reported here support this notion. First and foremost, transient docking, which appears to mirror the time course of paired-pulse facilitation (Kusick et al., 2020), is completely blocked in syt7 KO hippocampal neurons. Consequently, these synapses do not facilitate, instead depressing quickly and profoundly, suggesting that syt7-mediated docking is at least in part necessary for facilitation. Second, despite release probability not changing, docked vesicles are more severely depleted (~33% compared to wild type at 5 ms after an action potential) in syt7 KO both after single action potentials (this study) and high-frequency trains (Vevea 2021). This implies that vesicles are normally recruited by syt7 to the active zone continuously during the first 15 ms after stimulation in WT synapses. Third, in the absence of the asynchronous Ca^{2+} sensor Doc2α, the recovery of docked vesicles is significantly faster, nearly returning to baseline by 11 ms, suggesting that some vesicles docked by syt7 are fused by Doc2α. Although we cannot rule out the possibility that Doc2α works by docking and then fusing vesicles that are initially undocked, slowed train depression of synchronous release and faster docked vesicle replenishment in Doc2α KO suggests vesicles are still being recruited in the absence of Doc2α, but do not fuse asynchronously. Thus, these data show that syt7-mediated docking contributes to both AR and short-term plasticity. We tested our model for the sequential action of syt7 and Doc2α by conducting an epistasis experiment using DKO mice. Disruption of syt7 did not exacerbate the loss of AR in Doc2α KOs either after single stimuli or train stimulation. These findings are consistent with the idea that syt7 functions upstream of Doc2 in a common pathway, with the upstream step (transient docking) specifically during sustained activity (summarized in the model shown in Figure S7).

We emphasize that the two-step model does not apply to AR triggered by a single action potential (Figure S7). Rather, it is specifically required to support release after two or more action potentials in quick succession. Knocking out syt7 completely blocks transient docking but does not affect AR after single stimuli, implying that already-docked vesicles can fuse asynchronously. The inverse is true for Doc2α, which means that the second step (fusion) of AR can still be blocked without blocking the first step (activity-dependent docking). This is consistent with physiological and simulation data on two-step release, which predict that syt7 contributes appreciably to release only after a second action potential and becomes more prominent as high-frequency stimulation goes on (Miki et al., 2018). There will be exceptions to this model. For example, at granule cell synapses deleting syt7 substantially decreases AR (Turecek and Regehr, 2018). It will be interesting to test whether this is because two-step release is sometimes important after single stimuli, or, as in other secretory cell types (Bendahmane et al., 2020), syt7 is indeed able to act as a direct Ca^{2+} sensor for exocytosis in certain contexts.

Methods

All animal care was performed according to the National Institutes of Health guidelines for animal research with approval from the Animal Care and Use Committees at the Johns Hopkins University School of Medicine and the University of Wisconsin, Madison (Assurance Number: A3368-01). Both male and female syt7^{KO}, Doc2α^{KO}, and WT littermates were used.

Mice

Mouse lines used for this study were as follows:

- C57BL/6-*Syt7*^{tm1Nan} (Chakrabarti et al., 2003)
- C57BL/6-*DOC2a*^{em1Smoc} (Sakaguchi et al., 1999)

Neuronal cell culture

Doc2α and syt7 KO mice were maintained as heterozygotes, so that littermate controls could be used. These mice were bred, and postnatal day 0-1 pups were genotyped, with homozygotes for the null allele (-/-) and the wild-type allele (+/+) being used for culture. For iGluSnFR experiments, WT and KO hippocampal neurons were grown in mass culture for 14 DIV. In brief, hippocampi were dissected from mouse brains and digested for 25 min at 37 °C in 0.25% trypsin-EDTA (Corning). After mechanical dissociation, hippocampal neurons were plated on 12 mm glass coverslips pretreated with poly-D-lysine (Thermofisher). Neurons were cultured in Neurobasal A (GIBCO) based media with B27 (2%, Thermofisher) and GlutaMAX (2 mM, GIBCO) at 37 °C with 5% CO_2.

For high-pressure freezing and electron microscopy, cell cultures were prepared on 6-mm sapphire disks atop a feeder layer of astrocytes as previously described (Kusick et al., 2020). Astrocytes were harvested from cortices with treatment of trypsin (0.05%) for 20 min at 37 °C, followed by trituration and seeding on T-75 flasks containing DMEM supplemented with 10% FBS and 0.2% penicillin-streptomycin. After 2 weeks, astrocytes were plated on 6-mm sapphire disks (Technotrade Inc) coated with poly-D-lysine (1 mg/ml), collagen (0.6 mg/ml) and 17 mM acetic acid at a density of 13 x 103 cells/cm^2. Genotyping was performed either 1) after hippocampal dissection, using cortices lysed with 10 mM Tris-HCL pH8.0 and 100 mM NaCl in presence of 50 µg proteinase K, with hippocampi either left in Neurobasal A at 37 °C before switching to papain after or left in dissection medium (1% penicillin-streptomycin, 1 mM pyruvate, 10 mM HEPES, 3 mM glucose in HBSS) at 4 °C, or 2) using tail clips (alkaline lysis; Truett et al., 2000) of live mice, which were then sacrificed and dissected after genotyping was finished. We note that leaving the neurons in dissection medium at 4 °C results in more consistent cell health than Neurobasal A at 37 °C, particularly when hippocampi are left for several hours while genotyping is performed. Hippocampi were dissected under a

microscope and digested with 1) papain (0.5 mg/ml) and DNase (0.01%) in the dissection medium for 25 min at 37 °C with gentle perturbation every 5 min or 2) papain (0.5 mg/mL) in Neurobasal A with 200 rpm shaking. After trituration, neurons were seeded onto astrocyte feeder layers at density of 20 x 10^3 cells/cm^2 (75,000 per well) and cultured in Neurobasal A with 2% B27 and 2 mM at 37 °C with 5% CO_2. Before use, sapphire disks were carbon-coated with a "4" to indicate the side that cells are cultured on. Health of the cells, as indicated by de-adhered processes, floating dead cells, and excessive clumping of cell bodies, was assessed immediately before experiments.

Plasmids

-pF(UG) CamKII sf iGluSnFR A184V (Vevea and Chapman, 2020); Addgene #158769
-pF(UG) CamKII sf iGluSnFR S72A (Vevea et al., 2021)

Lentivirus production and use

For viral transduction, the original (Marvin et al., 2013; Vevea and Chapman, 2020) and low-affinity glutamate S72A were used (Marvin et al., 2018; Vevea et al., 2021). iGluSnFRs were subcloned into a FUGW transfer plasmid (Vevea and Chapman, 2020). Lentiviral particles were generated as previously described (Vevea and Chapman, 2020; Vevea et al., 2021) by co-transfecting the transfer, packaging, and helper (pCD/NL-BH*ΔΔΔ and VSV-G encoding pLTR-G) plasmids into HEK 293/T cells. Lentivirus was collected from the media 48–72 h after transfection and concentrated by ultracentrifugation. Viruses were titrated and then used to infect neurons on DIV 3-5.

iGluSnFR imaging and quantification

iGluSnFR fluorescence intensity changes were recorded as previously described (Vevea and Chapman, 2020; Vevea et al., 2021). To measure iGluSnFR signals in response to a single stimulus, the original high-affinity iGluSnFR was used in Figures 1A-E and S1. For train stimulation, the low affinity iGluSnFR sensor was used because it more effectively resolved individual responses from high-frequency stimulation due to its faster decay time (Vevea et al., 2021). Briefly, images were acquired, using 2x2 binning, in media (305 mOsm) comprising (in mM): 128 NaCl, 5 KCl, 2 $CaCl_2$, 1 $MgCl_2$, 30 D-glucose, and 25 HEPES, pH 7.3. For imaging experiments using a single stimulus, 200 frames were collected using 10 ms exposure times (2 sec total); a single field stimulus was applied 500 ms after the initial frame. For train stimulation experiments, 50 stimuli at 10 Hz (5 s) or 20 Hz (2.5 sec) were applied via field stimulation, and 500 or 750 frames, each with a 10 ms exposure time, were collected. Glutamate release signals were defined as fluorescence intensity changes that > five-times the standard deviation of the noise. For all iGluSnFR experiments, we initially recorded 500 ms as the baseline; the mean intensity was defined as F_0. iGluSnFR fluorescence amplitude

changes are reported as $\Delta F/F_0$. Throughout this study, we term regions of interest as boutons, because these regions were defined as yielding at least one iGluSnFR response during the first three stimuli of a 10 Hz train.

Brain slice preparation

Acute hippocampal slices were prepared from mice aged between P30 and P60. Animals were anesthetized using isoflurane and then rapidly decapitated. Brains were quickly removed and placed into ice-cold NMDG-HEPES artificial cerebral spinal fluid (aCSF; 300–310 mOsm) comprising (in mM): 92 N-Methyl-D-glucamine (NMDG), 2.5 KCl, 1.25 NaH_2PO_4, 30 $NaHCO_3$, 25 glucose, 2 thiourea, 5 Na-ascorbate, 3 Na-pyruvate, 0.5 $CaCl_2$, and 10 $MgSO_4$, and 20 HEPES, pH7.3. This solution was continuously bubbled with 95% O_2 and 5% CO_2. Three hundred µm thick coronal brain sections containing the hippocampal region were cut using a vibratome (Leica VT1200, Leica, Germany). To avoid any potential recurrent excitation, a sharp cut was made between CA3 and CA1. Slices were placed in a chamber and allowed to recover in 150 ml artificial cerebral spinal fluid at 34 °C for 25 min. Sodium (2 M stock in artificial cerebral spinal fluid) was added back at the following time intervals: 0 min (250 µl), 5 min (250 µl), 10 min (500 µl), 15 min (1 ml), and 20 min (2 ml) during the 25 min recovery incubation. Slices were then gently placed into another chamber containing aCSF but with 92 mM NMDG replaced with 92 mM NaCl, at room temperature (at least 1 hour) before being transferred to the recording chamber.

Electrophysiological recordings in acute hippocampal slices

Whole-cell voltage-clamp recordings were performed under an upright microscope (BX51WI, Olympus, Melville, NY) equipped with a water-immersion objective (LUMPlanFL N 40x/0.8 W; Olympus, Melville, NY). Hippocampal slices were continuously perfused (2 ml/min) with carbogen-saturated, modified aCSF (in mM: 125 NaCl, 25 $NaHCO_3$, 25 glucose, 2.5 KCl, 2 $CaCl_2$, 1.25 NaH_2PO4, and 1 $MgCl_2$, adjusted to 300-310mOsm). For perfusion, aCSF was heated to 34°C using a Single Channel Temperature Controller (TC-324C, Warner Instruments, Holliston, MA). Recording pipettes were prepared from borosilicate glass (1.5 mm diameter glass capillary, Sutter Instrument, Novato, CA) using a two-step puller (PP-830, Narishige, Japan), and were polished using an MF-830 micro forge (Narishige, Japan) immediately prior to use. Pipette position was controlled using an MP-285 motorized micromanipulator (Sutter Instrument, Novato, CA); the resistances were typically 4-6 MΩ when filled with recording solution consisting of (in mM): 135 K-gluconate 5 KCl, 10 HEPES, 1 EGTA, 6 Na_2 phosphocreatine, 0.3 Na_3GTP 2 MgATP. To chelate residual Ca2+, EGTA-AM (Millipore, Burlington, Massachusetts) was added to the bath at a final concentration of 25 µM for 30 minutes; neurons were then allowed to recover for another 20 minutes before being placed in the recording chamber. Neurons in the CA1 region were

visualized using a Retiga electro CCD camera (ELEDYNE PHOTOMETRICS, Tucson, AZ). Patched neurons were held at −70 mV, with access resistance (Ra) less than 20 MΩ throughout the recordings. A concentric bipolar electrode (FHC, 125/50 µm extended tip) was placed in the stratum radiatum (Schaffer collateral fiber) ~300-500 µm away from the recording pipette. EPSCs were pharmacologically isolated by bath application of 50 µM D-APV and 20 µM bicuculine. QX-314 chloride (5 mM) was in the pipette solution for evoked recordings. All data were collected in voltage-clamp mode using a Multiclamp 700B patch-clamp amplifier (Molecular Devices, San Jose, CA, USA) and a Digidata 1500B (Axon Digidata 1500B, Molecular Devices).

High-pressure freezing and freeze substitution

Cells cultured on sapphire disks were frozen using an EM ICE high-pressure freezer (Leica Microsystems), exactly as previously described(Kusick et al., 2020). The freezing apparatus was assembled on a table heated to 37 °C in a climate control box, with all solutions pre-warmed (37 ºC). Sapphire disks with neurons were carefully transferred from culture medium to a small culture dish containing physiological saline solution (140 mM NaCl, 2.4 mM KCl, 10 mM HEPES, 10 mM glucose; pH adjusted to 7.3 with NaOH, 300 mOsm). NBQX (3 µM; Tocris) and bicuculline (30 µM; Tocris) were added to the physiological saline solution to block recurrent synaptic activity. $CaCl_2$ and $MgCl_2$ concentrations were 1.2 mM and 3.8 mM, respectively. After freezing, samples were transferred under liquid nitrogen to an EM AFS2 freeze substitution system at -90 °C (Leica Microsystems). Using pre-cooled tweezers, samples were quickly transferred to anhydrous acetone at -90 °C. After disassembling the freezing apparatus, sapphire disks with cells were quickly moved to cryovials containing freeze substitution solutions. For the first two of three Syt7 knockout freezes, freeze substitution was performed exactly as previously described in (Kusick et al., 2020): solutions were 1% glutaraldehyde, 1% osmium tetroxide, and 1% water in anhydrous acetone, which had been stored under liquid nitrogen then moved to the AFS2 immediately before use. The freeze substitution program was as follows: −90 °C for 6-10 hr (adjusted so substitution would finish in the morning), 5 °C h^{-1} to −20 °C, 12 h at -20 °C, and 10 °C h^{-1} to 20 °C. For all other experiments, we used a different freeze substitution protocol that yields more consistent, high-contrast morphology, as described in (Vevea et al., 2021): samples were first left in 0.1% tannic acid and 1% glutaraldehyde at -90 °C for ~36 hours, then washed 5x, once every 30 min, with acetone, and transferred to 2% osmium tetroxide, then run on the following program: 11 hr at −90 °C, 5 °C h^{-1} to -20 °C, -20 °C for 12 hr, 10 °C h^{-1} to -4 °C, then removed from the freeze substitution chamber and warmed at room temperature for ~15 min before washing. For this latter protocol, instead of cryovials, solutions and sapphires were stored in universal sample containers (Leica Microsystems), covered in aclar film to prevent evaporation. Using these

containers instead of cryovials makes all solution transfers, from fixation through infiltration and embedding, much faster and more convenient.

Infiltration, embedding, sectioning, and transmission electron microscopy

Infiltration, embedding, and sectioning were performed as previously described (Kusick et al., 2020), except without en-bloc staining, which we found to not improve morphology. Samples in fixatives were washed three times, 10 min each, with anhydrous acetone, then left in 30% epon araldite (epon, 6.2 g; araldite, 4.4 g; DDSA, 12.2 g; and BDMA, 0.8 ml, diluted in acetone) for 3 h, then 70% epon araldite for 2 h, both with shaking. Samples were then transferred to caps of polyethylene BEEM capsules (EMS) and left in 90% epon araldite overnight at 4 °C. The next morning, samples were transferred to 100% epon araldite for 1 h, then again to 100% for 1 h, and finally transferred to 100% epon araldite and baked at 60 °C for 48 h.

For ultramicrotomy, 40-nm sections were cut. Sections on single-slot grids coated with 0.7% pioloform were stained with 2.5% uranyl acetate then imaged either at 120 kV on the 57,000x setting on a Thermo-Fisher Talos L120C equipped with a Ceta camera (pixel size = 244 pm; first replicate of the Doc2 experiment) or at 80 kV on the 100,000x setting on a Hitachi 7600 TEM equipped with an AMT XR50 camera run on AMT Capture v6 (pixel size = 560 pm, all other experiments). Samples were blinded before imaging. To further limit bias, synapses were found by bidirectional raster scanning along the section at the magnification at which images were taken, which makes it difficult to “pick” certain synapses, as a single synapse takes up most of this field of view. Synapses were identified by a vesicle-filled presynaptic bouton and a postsynaptic density. Postsynaptic densities are often subtle in our samples, but synaptic clefts were also identifiable by 1) their characteristic width, 2) the apposed membranes following each other closely, and 3) vesicles near the presynaptic active zone. 125-150 micrographs per sample of anything that appeared to be a synapse were taken without close examination. All images were from different synapses (that is, images were never captured from different sections of the same synapse). Most of the time all images for a condition were taken from a single section, each of which typically contains hundreds of different boutons; when different sections were used, they were always at least 10 serial sections apart (400 nm in z) to ensure they didn’t contain any of the same boutons.

Electron microscopy image analysis

EM image analysis was performed as previously described (Kusick et al., 2020). All the images from a single experiment were randomized for analysis as a single pool. Only after this randomization were any images excluded from analysis, either because they appeared to not contain a bona fide synapse, or the morphology was too poor for

reliable annotation. The PM, the active zone, docked SVs, and all SVs in the bouton were annotated in ImageJ using SynapsEM plugins (Watanabe et al., 2020) [https://github.com/shigekiwatanabe/SynapsEM copy archived at swh:1:rev:11a6227cd5951bf5e077cb9b3220553b506eadbe]. The active zone was identified as the region of the presynaptic PM with the features described above for identifying a synapse. Docked vesicles were identified by their membrane appearing to be in contact with the PM at the active zone (0 nm from the PM); that is, there are no lighter pixels between the membranes. Vesicles that were not manually annotated as docked but were 0 nm away from the active zone PM were automatically counted as docked when segmentation was quantitated (see below) for data sets counting the number of docked vesicles. Likewise, vesicles annotated as docked were automatically placed in the 0 nm bin of vesicle distances from the PM. To minimize bias and error, and to maintain consistency, all image segmentation, still in the form of randomized files, was thoroughly checked and edited by a second member of the lab. Features were then quantitated using the SynapsEM (Watanabe et al., 2020) family of MATLAB (MathWorks) scripts (https://github.com/shigekiwatanabe/SynapsEM). Example electron micrographs shown were adjusted in brightness and contrast to different degrees (depending on the varying brightness and contrast of the raw images), rotated, and cropped in ImageJ before import into Adobe Illustrator.

Statistics

Statistical analysis was performed using GraphPad Prism 9 software. iGluSnFR and electrophysiology data were presented as mean ± standard error of the mean. Electron microscopy data were presented as mean and 95% confidence interval of the mean. For iGluSnFR and electrophysiology, data sets were tested for normality using the Anderson-Darling test and corresponding parametric or non-parametric hypothesis tests performed, as stated in the figure legends. Since electron microscopy pit and docked vesicle data are count data, following a roughly binomial rather than normal distribution, means were used to graph the data (medians are not a useful representation of central tendency for count data, particularly low-frequency count data. For example the median number of pits in all samples is 0 since exocytic pits are rare) and Games-Howell post-hoc test used, which does not assume a normal distribution.

Data availability

Full data tables underlying the Figures 5 and 6 are available in the source data. Raw images and image analysis files are available upon request.

Code availability

Custom R, Matlab and Fiji scripts for electron microscopy analysis are available at https://github.com/shigekiwatanabe/SynapsEM. More details can be found in (Watanabe et al., 2020)

Figure legends

Figure 1. Doc2α, and not syt7, drives most of the asynchronous glutamate release triggered by a single action potential in cultured hippocampal neurons.
(A) Representative images showing an iGluSnFR response following a single stimulus; scale bar, 5 μm. Glutamate binding induces conformational changes in the sensor, resulting in increases in the fluorescence intensity from the GFP moiety (green cylinder; (Marvin et al., 2013))
(B) Color coding and binning the temporal changes in iGluSnFR signals within 70 ms after a single stimulus for WT (n=15; from 4 independent litters), Doc2α^{KO} (n=17; from 5 independent litters), syt7^{KO} (n=15; from 4 independent litters), and EGTA-AM treated neurons (n=18; from 4 independent litters). The temporal color code is red (initiation of stimulus) to purple (70 ms after the stimulus); scale bar, 5 μm. Histograms of iGluSnFR ($\Delta F/F_0$) peaks were generated using 10 ms binning. Samples were color-coded as follows: WT (gray), Doc2α^{KO} (reddish), syt7^{KO} (cyan), and EGTA-AM (orange) treated neurons. The histograms include donut graph insets to display the fraction of release in each bin.
(C) Violin plot showing the % AR (>10 ms) for each condition. One-way ANOVA, followed by Dunnett's test, was used to compare mutants against WT. *** indicates $p<0.001$.
(D) Average iGluSnFR signals from WT, Doc2α^{KO}, syt7^{KO}, and EGTA-AM treated neurons (left), and the corresponding normalized cumulative plot of these same data (right).
(E) Bar graphs showing that loss of Doc2α or treatment with EGTA-AM results in significant reductions in AR. EGTA-AM also resulted in small, but significant, decrease in the fast t value. One-way ANOVA, followed by Dunnett's test to compare mutants against WT, was performed. * indicates $p<0.05$, *** indicates $p<0.001$.

Figure 2. Doc2α, and not syt7, drives most of the AR triggered by a single action potential at Schaffer collaterals.
(A) Schematic of the recording scheme of hippocampal slices showing stimulation of the Schaffer collateral fibers and whole-cell patch clamp recordings of CA1 pyramidal neurons.
(B) Averaged traces of evoked EPSCs recorded from WT (n=18; from 5 independent litters), Doc2α^{KO} (n=15; from 4 independent litters), syt7^{KO} (n=19; from 6 independent litters), and EGTA-AM treated neurons (n=20; from 4 independent litters).

(C) Normalized cumulative EPSC charge transfer over 400 ms.
(D) Bar graphs, from corresponding groups in panels (B-C), summarizing the amplitude, fast and slow EPSC charge, and the fast and slow EPSC t values. One-way ANOVA, followed by Dunnett's test, was used to compare mutants against WT. **, and *** indicate $p< 0.01$, and $p<0.001$.

Figure 3. Both Doc2α and syt7 contribute to asynchronous glutamate release during train stimulation but have opposite effects on short-term plasticity at in cultured hippocampal neurons.
(A) Representative iGluSnFR images from trains of 50 APs at 10 Hz (left) or 20 Hz (right). Images on the left, middle and right each show a sum of 20 frames (200 msec) before, during, and after stimulation, respectively; scale bar, 40 µm.
(B) Representative iGluSnFR responses from WT (n=12; from 3 independent litters), Doc2α^{KO} (n=14; from 4 independent litters), and syt7^{KO} neurons (n=15; from 3 independent litters), stimulated at 10 Hz (top) and 20 Hz (bottom).
(C) Plot of the cumulative iGluSnFR signals, after discarding the synchronous release during the first 10 msec, showing that Doc2α^{KO} neurons exhibit significant reductions in AR when neurons are stimulated at either 10 or 20 Hz. The insets show the first three data points on an expanded scale.
(D) Plot of the normalized amplitude of iGluSnFR signals evoked by 50 stimuli at 10 and 20 Hz. Insets show the first three points of each trace on expanded scales.

Figure 4. Both Doc2α and syt7 contribute to AR during train stimulation but have opposite effects on short-term plasticity at Schaffer collaterals.
(A) Representative EPSCs triggered by 20 Hz stimulus trains using WT, Doc2α^{KO}, syt7^{KO}, and EGTA-AM treated neurons. The shaded gray areas indicate the tonic charge component that likely corresponds to AR.
(B) The peak amplitude of each EPSC during the train was normalized to the first EPSC from WT (n=12; from 4 independent litters), Doc2α^{KO} (n=11; from 3 independent litters), syt7^{KO} (n=10; from 3 independent litters), and EGTA-AM treated neurons (n=11, from 3 independent litters).
(C) Cumulative asynchronous charge transfer from WT, Doc2a^{KO}, syt7^{KO}, and EGTA-AM treated CA1 hippocampal neurons. The asynchronous component was isolated by taking a 20-50 ms time window from each individual EPSC.

Figure 5. Doc2α, but not syt7, is required for asynchronous synaptic vesicle fusion triggered by a single action potential in cultured hippocampal neurons.
(A-D) Example transmission electron micrographs of syt7^{WT} (A), syt7^{KO} (B), Doc2α^{WT} (C), and Doc2α^{KO} (D) synapses frozen at the indicated time points after an action

potential (AP) or without stimulation (no stim). Arrows indicate pits in the active zone, which are presumed to be synaptic vesicles that have fused with the plasma membrane. (E) The number of pits in the active zone per synaptic profile (part of the synapse captured in a 2D section) in syt7 wild-type littermate controls and knockouts. Error bars indicate 95% confidence interval of the mean for all data pooled together; each dot indicates the mean from a single biological replicate. Inset: same data from the 11 ms time point from each genotype, with lesser y axis range; lines indicate data are from the same biological replicate (experiment), *not* that they are paired. *P* values are from comparisons between wild-type controls (no stim, $n = 217$; 5 ms, $n = 216$; 11 ms, $n = 217$; 14 ms, $n = 230$ synaptic profiles) and knockouts (no stim, $n = 193$; 5 ms, $n = 215$; 11 ms, $n = 230$; 14 ms, $n = 212$ synaptic profiles) frozen at the same time point.
(F) same as E, but for Doc2α wild-type controls (no stim, $n = 327$; 5 ms, $n = 229$; 11 ms, $n = 336$; 14 ms, $n = 192$ synaptic profiles) and knockouts (no stim, $n = 330$; 5 ms, $n = 231$; 11 ms, $n = 352$; 14 ms, $n = 321$ synaptic profiles).
Number of biological replicates (from separate cultures frozen on different days and analyzed in separate randomized batches): 2 for each of the syt7 time points, 2 for 5 ms and 14 ms Doc2 WT, 2 for 5 ms and 11 ms Doc2 KO, 3 for Doc2 WT no stim and 11 ms, 3 for Doc2 KO no stim and 14 ms. The numbers of pits between wild type and knockout were compared using Brown-Forsythe ANOVAs with post-hoc Games-Howell's multiple comparisons tests. In pairwise tests, the same time point for wild type vs. knockout as well as each time point within each genotype were compared against each other (only comparisons between the same time point for wild type vs. knockout are shown, see Supplementary Table 1 for all pairwise comparisons). See Source Data 1 for data used to generate the graphs shown. See Figure S5A for active zone sizes from each condition and Figure S5B for pit data normalized to the size of active zones.

Figure 6. Syt7, is absolutely required for transient docking, while docked vesicles recover more quickly without Doc2α.
(A-D) Example transmission electron micrographs of syt7^{WT} (A), syt7^{KO} (B), Doc2α^{WT} (C), and Doc2α^{KO} (D) synapses frozen at the indicated time points after an action potential (AP) or without stimulation (no stim). Arrows indicate docked vesicles (synaptic vesicles with no visible distance between their membrane and the plasma membrane).
(E) The number of docked vesicles per synaptic profile (part of the synapse captured in a 2D section) in syt7 wild-type littermate controls and knockouts. Error bars indicate 95% confidence interval of the mean for all data pooled together; each dot indicates the mean from a single biological replicate. *P* values are from comparisons between wild-type controls (no stim, $n = 217$; 5 ms, $n = 216$; 11 ms, $n = 217$; 14 ms, $n = 230$ synaptic profiles) and knockouts (no stim, $n = 193$; 5 ms, $n = 215$; 11 ms, $n = 230$; 14 ms, $n = 212$ synaptic profiles) frozen at the same time point.

(F) same as E, but for Doc2α wild-type controls (no stim, $n = 327$; 5 ms, $n = 229$; 11 ms, $n = 336$; 14 ms, $n = 192$ synaptic profiles) and knockouts (no stim, $n = 330$; 5 ms, $n = 231$; 11 ms, $n = 352$; 14 ms, $n = 321$ synaptic profiles).
Number of biological replicates (from separate cultures frozen on different days and analyzed in separate randomized batches): 2 for each of the syt7 time points, 2 for 5 ms and 14 ms Doc2 WT, 2 for 5 ms and 11 ms Doc2 KO, 3 for Doc2 WT no stim and 11 ms, 3 for Doc2 KO no stim and 14 ms. The numbers of pits between wild type and knockout were compared using Brown-Forsythe ANOVAs with post-hoc Games-Howell's multiple comparisons tests. In pairwise tests, the same time point for wild type vs. knockout as well as each time point within each genotype were compared against each other (only comparisons between the same time point for wild type vs. knockout are shown, see Supplementary Table 1 for all pairwise comparisons). See Source Data 2 for data used to generate the graphs shown. See Figure S5A for active zone sizes from each condition, Figure S5C for docked vesicle data normalized to the size of active zones, and Figure S5D for distribution of undocked vesicles.

Figure 7. AR in Doc2α/syt7 DKO neurons: non-additive effects on AR indicate function through a common pathway.
All recordings were carried out using acute hippocampal slices, in CA1, as described in Figures 2 and 4.
(A) Averaged traces of evoked EPSCs recorded from WT (n=18; from 5 independent litters), Doc2αKO (n=15; from 4 independent litters), Doc2α/syt7 DKO (n=14; from 4 independent litters), and EGTA-AM treated neurons (n=20; from 4 independent litters).
(B) Bar graph summarizing the slow EPSC charge values. One-way ANOVA, followed by Dunnett's test, was used to compare mutants against WT. **, and *** indicate $p< 0.01$, and $p<0.001$.
(C) Representative EPSCs triggered by 20 Hz stimulus trains using WT and Doc2α/syt7 DKO (n=15; from 5 independent litters) neurons.
(D) Cumulative asynchronous charge transfer from WT, Doc2αKO, syt7KO, Doc2a/syt7 DKO, and EGTA-AM treated neurons.

Figure S1. Expression of iGluSnFR in cultured hippocampal neurons.
(A) Representative serial frames of iGluSnFR fluorescence from the WT, Doc2α^{KO}, and syt7^{KO} neurons, before and after eliciting a single action potential (AP; arrow); the heatmap is shown on the right.

Figure S2. Spatial distribution of AR, measured via iGluSnFR imaging, in cultured hippocampal neurons.
(A) Schematic illustrating AR distribution patterns at axon terminals; the large shaded grey circles depict the soma; small circles depict presynaptic boutons. For this analysis,

only AR was analyzed, using data collected from 923 ROIs that were initially identified because they yielded at least one evoked response (AR, synchronous, or both) in the first three stimuli from a 10 Hz train. Boutons that exhibit AR, for the indicated position and stimulus, are orange; open circles indicate boutons that did not exhibit AR at the indicated position or stimulus. All of the AR distribution patterns in each of the four sub-panels are from the same boutons at the same fixed positions. For convenience, only twelve boutons are shown, and these are numbered 1-12 to emphasize that the same boutons are analyzed in each of the sub-panels. The organization of these boutons was artificially grouped to some extent, to better visualize the patterns of release between each stimulus. The bottom left table quantifies the ratio of AR patterns: AR to AR, AR to no AR, no AR to AR, and no AR to no AR, from the first to the second stimulus. The same analysis, but between the second and third stimulus, is provided in the bottom right table. The distribution of AR to target cells in the first versus the second pulses is similar to the distribution between the third and fourth pulses. These data suggest that AR during the first pulse, while molecularly distinct, does not segregate to different target cells, as compared to AR elicited by subsequent stimuli.
(B) Table summarizing the fraction of boutons with the same responses after the initial three stimuli. AR only; represents pure AR that successively occurred three times at the same bouton, in the absence of SR. Synchronous release (SR) only; indicates boutons that exhibited purely SR during the first three stimuli, in the absence of AR. AR; reflects AR that occurred at the same bouton for all three successive stimuli regardless of the presence or absence of SR. Interpretation: In the main text we noted that spatial segregation of AR during the first two responses was not observed. Expanding on this further, the same pattern was observed when comparing the second and third responses. Moreover, nearly 70% of all responding boutons exhibited AR at least once during the first three stimuli in a train, either with or without a concurrent synchronous component (panel 2A). So, even though AR presents only a third of the charge transfer in our experiments (Figures 1C,E, and 2D), this mode of release is widespread. In addition, 40% of all responding boutons analyzed exhibited AR in all three of the initial stimuli in a train, and approximately half of the boutons that had AR after the first stimulus also yielded AR during the second stimulus (panel 2B). In contrast, only 6% and 8% of boutons exhibited pure AR or synchronous responses, respectively, in response to all three initial stimuli in a train (panel 2B). While our data argue against the segregation of AR during the first response, it remains possible that further analysis, of much larger data sets, using sensitive algorithms, could reveal more subtle differences that might have escaped detection.

Figure S3. AR in acute brain slices from Doc2α and syt7 KO mice during 10 Hz train stimulation.
(A) Representative hippocampal slice from a WT mouse.

(B) A stimulating electrode was placed in the Schaffer collateral pathway and transmission to CA1 neurons was monitored via whole-cell patch clamp recordings.
(C), (D) Same as Figure 4B,C, but using 10 Hz stimulation instead of 20 Hz stimulation. The data show synaptic depression and asynchronous responses from WT (n=15; from 3 independent litters), Doc2α^{KO} (n=18; from 5 independent litters), syt7^{KO} (n=14; from 3 independent litters), and EGTA-AM-treated WT neurons (n=12; from 3 independent litters).

Figure S4. Additional example transmission electron micrographs.

Figure S5. Additional quantification from electron microscopy.
(A) Size of the active zone in each synaptic profile from each condition. Each dot indicates a single synaptic profile. Error bars: median and interquartile range.
(B) Same pit data from Figure 5, normalized to the size of the active zone in each condition. "Per 500 nm of active zone" calculation was performed by multiplying the count from each synaptic profile by 500 and dividing by the mean active zone size from the data set (i.e., normalization was not performed by the size of the active zone in each individual synaptic profile).
(C) Same as B, but for docked vesicle data from Figure 6.
(D) Distances of undocked synaptic vesicles from the plasma membrane at the active zone, not including docked vesicles (which are 0 nm from the plasma membrane). Distances are binned in 5-nm increments ("5" indicates vesicles 0.1–5 nm from the membrane, "10" indicates 6–10 nm, and so on). Each dot indicates the mean number of synaptic vesicles per synaptic profile in that distance range from the active zones. See Source Data 3 for data used to generate the graphs.

Figure S6. Synaptic depression of phasic responses in Doc2α/syt7 DKOs, compared to single KO and AM-EGTA treated conditions.
Recordings of CA1 neurons in hippocampal slices were carried out as described in Figure 4. The peak amplitude of each EPSC during 50 APs at 20Hz was normalized to the first EPSC from Doc2α/syt7 DKO slices; for comparison, all other conditions were replotted from Figure 4. As predicted, the depression phenotype of the DKO lies between the Doc2α and syt7 depression curves but mimics the syt7 KO by the end of the train.

Figure S7. Doc2α triggers AR in response to single action potentials; during repetitive stimulation, syt7 mediates transient docking to feed docked vesicles to Doc2α for ongoing AR.
At rest, SVs are docked at the active zone (solid gray line) in a dynamic equilibrium indicated by the antiparallel black arrows (far left panel). Under these conditions,

docking is not affected by syt7 (Figure 6E; Vevea et al. (2021). A single action potential triggers both undocking (UD) and synchronous release (SR), resulting in a 40% reduction in docked vesicles in ~5 ms (Figure 6E,F; Kusick et al., 2020). This is followed by a transient docking (TD) step in which vesicles re-attach to the active zone via a process that takes 14 msec and is mediated by Ca^{2+} and syt7 (granite green) (Figure 6E,F; Kusick et al., 2020;). The same single AP also triggers AR mediated directly by Doc2α (lilac), at the 11 ms time point (Figure 5F; Yao et al., 2011). Syt7 plays no role in release during the first action potential (Figures 1,2, and 5E; and references in the main text), again because it does not regulate docking in the resting state. However, loss of syt7 abolishes activity-dependent TD (Figure 6E), which decreases the availability of docked vesicles during subsequent (i.e., two or more) action potentials, indirectly reducing Doc2α–triggered AR during ongoing activity. As a test of this model, an epistasis experiment revealed that the Doc2α/syt7 DKO AR phenotype was non-additive (Figure 7). This validates a sequential, two-step, model, in which—during ongoing activity—syt7 feeds docked vesicles to Doc2α, which directly mediates AR. Hence, syt7 acts upstream of Doc2α, as a docking factor, while Doc2α functions as the proximal Ca^{2+} sensor for AR in hippocampal synapses. This model can account for why only Doc2α drives AR in response to a single action potential, while Doc2α and syt7 contribute equally to AR during subsequent action potentials.

References

Bacaj, T., Wu, D., Yang, X., Morishita, W., Zhou, P., Xu, W., Malenka, R.C., and Südhof, T.C. (2013). Synaptotagmin-1 and Synaptotagmin-7 Trigger Synchronous and Asynchronous Phases of Neurotransmitter Release. Neuron *80*, 947–959.

Bendahmane, M., Morales, A., Kreutzberger, A.J.B., Schenk, N.A., Mohan, R., Bakshi, S., Philippe, J.M., Zhang, S., Kiessling, V., Tamm, L.K., et al. (2020). Synaptotagmin-7 enhances calcium-sensing of chromaffin cell granules and slows discharge of granule cargos. J. Neurochem. *154*, 598–617.

Blanchard, K., Zorrilla, J., Mart, D.S., Marty, A., Llano, I., and Trigo, F.F. (2020). Differentially poised vesicles underlie fast and slow components of release at single synapses. J. Gen. Physiol. *152*.

Chakrabarti, S., Kobayashi, K.S., Flavell, R.A., Marks, C.B., Miyake, K., Liston, D.R., Fowler, K.T., Gorelick, F.S., and Andrews, N.W. (2003). Impaired membrane resealing and autoimmune myositis in synaptotagmin VII-deficient mice. J. Cell Biol. *162*, 543–549.

Chang, S., Trimbuch, T., and Rosenmund, C. (2018). Synaptotagmin-1 drives synchronous Ca2+-triggered fusion by C2B-domain-mediated synaptic-vesicle-membrane attachment. Nat. Neurosci. *21*, 33–42.

Chen, C., and Regehr, W.G. (1999). Contributions of residual calcium to fast synaptic transmission. J. Neurosci. *19*, 6257–6266.

Chen, C., Satterfield, R., Young, S.M., Jonas, P., Chen, C., Satterfield, R., Young, S.M., and Jonas, P. (2017). Triple Function of Synaptotagmin 7 Ensures

Efficiency of High-Frequency Transmission at Central GABAergic Synapses. Cell Rep. *21*, 2082–2089.

Deng, S., Li, J., He, Q., Zhang, X., Zhu, J., Li, L., Mi, Z., Yang, X., Jiang, M., Dong, Q., et al. (2020). Regulation of Recurrent Inhibition by Asynchronous Glutamate Release in Neocortex. Neuron *105*, 522-533.e4.

Gaffaney, J.D., Xue, R., Chapman, E.R., and Brennwald, P.J. (2014). Mutations that disrupt Ca 2 + -binding activity endow Doc2 β with novel functional properties during synaptic transmission. Mol. Biol. Cell *25*, 481–494.

Goda, Y., and Stevens, C.F. (1994). Two components of transmitter release at a central synapse. Proc. Natl. Acad. Sci. *91*, 12942–12946.

Groffen, A.J., Martens, S., Arazola, R.D., Cornelisse, L.N., Lozovaya, N., de Jong, A.P.H., Goriounova, N.A., Habets, R.L.P., Takai, Y., Borst, J.G., et al. (2010). Doc2b Is a High-Affinity Ca2+ Sensor for Spontaneous Neurotransmitter Release. Science (80-.). *327*, 1614–1618.

Hui, E., Bai, J., Wang, P., Sugimori, M., Llinas, R.R., and Chapman, E.R. (2005). Three distinct kinetic groupings of the synaptotagmin family: candidate sensors for rapid and delayed exocytosis. Proc. Natl. Acad. Sci. U. S. A. *102*, 5210–5214.

Huson, V., and Regehr, W.G. (2020). Diverse roles of Synaptotagmin-7 in regulating vesicle fusion. Curr. Opin. Neurobiol. *63*, 42–52.

Iremonger, K.J., and Bains, J.S. (2007). Integration of Asynchronously Released Quanta Prolongs the Postsynaptic Spike Window. J. Neurosci. *27*, 6684–6691.

Jackman, S.L., and Regehr, W.G. (2017). The Mechanisms and Functions of Synaptic Facilitation. Neuron *94*, 447–464.

Jackman, S.L., Turecek, J., Belinsky, J.E., and Regehr, W.G. (2016). The calcium sensor synaptotagmin 7 is required for synaptic facilitation. Nature *529*, 88–91.

Jiang, M., Zhu, J., Liu, Y., Yang, M., Tian, C., Jiang, S., Wang, Y., Guo, H., Wang, K., and Shu, Y. (2012). Enhancement of asynchronous release from fast-spiking interneuron in human and rat epileptic neocortex. PLoS Biol. *10*.

Kaeser, P.S., and Regehr, W.G. (2014). Molecular mechanisms for synchronous, asynchronous, and spontaneous neurotransmitter release. Annu. Rev. Physiol. *76*, 333–363.

Khan, M.M., and Regehr, W.G. (2020). Loss of doc2b does not influence transmission at purkinje cell to deep nuclei synapses under physiological conditions. Elife *9*, 1–13.

Kusick, G.F., Chin, M., Raychaudhuri, S., Lippmann, K., Adula, K.P., Hujber, E.J., Vu, T., Davis, M.W., Jorgensen, E.M., and Watanabe, S. (2020). Synaptic vesicles transiently dock to refill release sites. Nat. Neurosci. *23*, 1329–1338.

Kusick, G.F., Ogunmowo, T.H., and Watanabe, S. (2022). Transient docking of synaptic vesicles: Implications and mechanisms. Curr. Opin. Neurobiol. *74*.

Li, S., Raychaudhuri, S., Lee, S.A., Brockmann, M.M., Wang, J., Kusick, G., Prater, C., Syed, S., Falahati, H., Ramos, R., et al. (2021). Asynchronous release sites align with NMDA receptors in mouse hippocampal synapses. Nat. Commun. *12*, 1–13.

Liu, H., Bai, H., Hui, E., Yang, L., Evans, C.S., Wang, Z., Kwon, S.E., and Chapman, E.R. (2014). Synaptotagmin 7 functions as a Ca2+-sensor for synaptic vesicle replenishment. Elife.

Manseau, F., Marinelli, S., Méndez, P., Schwaller, B., Prince, D.A., Huguenard,

J.R., and Bacci, A. (2010). Desynchronization of neocortical networks by asynchronous release of GABA at autaptic and synaptic contacts from fast-spiking interneurons. PLoS Biol. *8*.

Marvin, J.S., Borghuis, B.G., Tian, L., Cichon, J., Harnett, M.T., Akerboom, J., Gordus, A., Renninger, S.L., Chen, T.W., Bargmann, C.I., et al. (2013). An optimized fluorescent probe for visualizing glutamate neurotransmission. Nat. Methods *10*, 162–170.

Marvin, J.S., Scholl, B., Wilson, D.E., Podgorski, K., Kazemipour, A., Mueller, J.A., Schoch-McGovern, S., Wang, S.S.-H., Urra Quiroz, F.J., Rebola, N., et al. (2018). Stability, affinity and chromatic variants of the glutamate sensor iGluSnFR. Nat. Methods *15*.

Maximov, A., Lao, Y., Li, H., Chen, X., Rizo, J., Sorensen, J.B., and Sudhof, T.C. (2008). Genetic analysis of synaptotagmin-7 function in synaptic vesicle exocytosis. Proc Natl Acad Sci U S A *105*, 3986–3991.

Miki, T., Malagon, G., Pulido, C., Llano, I., Neher, E., and Marty, A. (2016). Actin- and Myosin-Dependent Vesicle Loading of Presynaptic Docking Sites Prior to Exocytosis. Neuron *91*, 808–823.

Miki, T., Nakamura, Y., Malagon, G., Neher, E., and Marty, A. (2018). Two-component latency distributions indicate two-step vesicular release at simple glutamatergic synapses. Nat. Commun.

Neher, E., and Brose, N. (2018). Dynamically Primed Synaptic Vesicle States: Key to Understand Synaptic Short-Term Plasticity. Neuron *100*, 1283–1291.

Otsu, Y., Shahrezaei, V., Li, B., Raymond, L.A., Delaney, K.R., and Murphy, T.H. (2004). Competition between Phasic and Asynchronous Release for Recovered Synaptic Vesicles at Developing Hippocampal Autaptic Synapses. J. Neurosci. *24*, 420–433.

Sabatini, B.L., and Regehr, W.G. (1996). Timing of neurotransmission at fast synapses in the mammalian brain. Nature *384*, 170–172.

Sakaguchi, G., Manabe, T., Kobayashi, K., Orita, S., Sasaki, T., Naito, A., Maeda, M., Igarashi, H., Katsuura, G., Nishioka, H., et al. (1999). Doc2α is an activity-dependent modulator of excitatory synaptic transmission. Eur. J. Neurosci. *11*, 4262–4268.

Silva, M., Tran, V., and Marty, A. (2021). Calcium-dependent docking of synaptic vesicles. Trends Neurosci. *44*, 579–592.

Stevens, C.F., and Sullivan, J.M. (2003). The synaptotagmin C2A domain is part of the calcium sensor controlling fast synaptic transmission. Neuron *39*, 299–308.

Truett, G.E., Heeger, P., Mynatt, R.L., Truett, A.A., Walker, J.A., and Warman, M.L. (2000). Preparation of PCR-quality mouse genomic dna with hot sodium hydroxide and tris (HotSHOT). Biotechniques *29*, 52–54.

Turecek, J., and Regehr, W.G. (2019). Neuronal Regulation of Fast Synaptotagmin Isoforms Controls the Relative Contributions of Synchronous and Asynchronous Release. Neuron *101*.

Turecek, J., and Regehr, X.W.G. (2018). Synaptotagmin 7 Mediates Both Facilitation and Asynchronous Release at Granule Cell Synapses. J. Neurosci. *38*, 3240–3251.

Vevea, J.D., and Chapman, E.R. (2020). Acute disruption of the synaptic vesicle

membrane protein synaptotagmin 1 using knockoff in mouse hippocampal neurons. Elife *9*, 1–24.

Vevea, J.D., Kusick, G.F., Chen, E., Courtney, K.C., Watanabe, S., and Chapman, E.R. (2021). Synaptotagmin 7 is enriched at the plasma membrane through γ-secretase processing to promote vesicle docking and control synaptic plasticity in mouse hippocampal neurons. Elife.

Watanabe, S., Davis, M.W., Kusick, G.F., Iwasa, J., and Jorgensen, E.M. (2020). SynapsEM: computer-assisted synapse morphometry. Front. Synaptic Neurosci.

Wen, H., Linhoff, M.W., Mcginley, M.J., Li, G., Corson, G.M., Mandel, G., and Brehm, P. (2010). Distinct roles for two synaptotagmin isoforms in synchronous and asynchronous transmitter release at zebra fish neuromuscular junction. Proc. Natl. Acad. Sci. *107*, 13906–13911.

Xue, R., Gaffaney, J.D., and Chapman, E.R. (2015). Structural elements that underlie Doc2β function during asynchronous synaptic transmission. Proc. Natl. Acad. Sci. *112*, E4316–E4325.

Xue, R., Ruhl, D.A., Briguglio, J.S., Figueroa, A.G., Pearce, R.A., and Chapman, E.R. (2018). Doc2-mediated superpriming supports synaptic augmentation. Proc. Natl. Acad. Sci. U. S. A. *115*, E5605–E5613.

Yao, J., Gaffaney, J.D., Kwon, S.E., and Chapman, E.R. (2011). Doc2 is a Ca 2+ sensor required for asynchronous neurotransmitter release. Cell *147*, 666–677.

Bacaj, T., Wu, D., Yang, X., Morishita, W., Zhou, P., Xu, W., Malenka, R.C., and Südhof, T.C. (2013). Synaptotagmin-1 and Synaptotagmin-7 Trigger Synchronous and Asynchronous Phases of Neurotransmitter Release. Neuron *80*, 947–959.

Bendahmane, M., Morales, A., Kreutzberger, A.J.B., Schenk, N.A., Mohan, R., Bakshi, S., Philippe, J.M., Zhang, S., Kiessling, V., Tamm, L.K., et al. (2020). Synaptotagmin-7 enhances calcium-sensing of chromaffin cell granules and slows discharge of granule cargos. J. Neurochem. *154*, 598–617.

Blanchard, K., Zorrilla, J., Mart, D.S., Marty, A., Llano, I., and Trigo, F.F. (2020). Differentially poised vesicles underlie fast and slow components of release at single synapses. J. Gen. Physiol. *152*.

Chakrabarti, S., Kobayashi, K.S., Flavell, R.A., Marks, C.B., Miyake, K., Liston, D.R., Fowler, K.T., Gorelick, F.S., and Andrews, N.W. (2003). Impaired membrane resealing and autoimmune myositis in synaptotagmin VII-deficient mice. J. Cell Biol. *162*, 543–549.

Chang, S., Trimbuch, T., and Rosenmund, C. (2018). Synaptotagmin-1 drives synchronous Ca2+-triggered fusion by C2B-domain-mediated synaptic-vesicle-membrane attachment. Nat. Neurosci. *21*, 33–42.

Chen, C., and Regehr, W.G. (1999). Contributions of residual calcium to fast synaptic transmission. J. Neurosci. *19*, 6257–6266.

Chen, C., Satterfield, R., Young, S.M., Jonas, P., Chen, C., Satterfield, R., Young, S.M., and Jonas, P. (2017). Triple Function of Synaptotagmin 7 Ensures Efficiency of High-Frequency Transmission at Central GABAergic Synapses. Cell Rep. *21*, 2082–2089.

Deng, S., Li, J., He, Q., Zhang, X., Zhu, J., Li, L., Mi, Z., Yang, X., Jiang, M., Dong, Q., et al. (2020). Regulation of Recurrent Inhibition by Asynchronous Glutamate Release in Neocortex. Neuron *105*, 522-533.e4.

Gaffaney, J.D., Xue, R., Chapman, E.R., and Brennwald, P.J. (2014). Mutations that disrupt Ca 2 + -binding activity endow Doc2 β with novel functional properties during synaptic transmission. Mol. Biol. Cell *25*, 481–494.

Goda, Y., and Stevens, C.F. (1994). Two components of transmitter release at a central synapse. Proc. Natl. Acad. Sci. *91*, 12942–12946.

Groffen, A.J., Martens, S., Arazola, R.D., Cornelisse, L.N., Lozovaya, N., de Jong, A.P.H., Goriounova, N.A., Habets, R.L.P., Takai, Y., Borst, J.G., et al. (2010). Doc2b Is a High-Affinity Ca2+ Sensor for Spontaneous Neurotransmitter Release. Science (80-.). *327*, 1614–1618.

Hui, E., Bai, J., Wang, P., Sugimori, M., Llinas, R.R., and Chapman, E.R. (2005). Three distinct kinetic groupings of the synaptotagmin family: candidate sensors for rapid and delayed exocytosis. Proc. Natl. Acad. Sci. U. S. A. *102*, 5210–5214.

Huson, V., and Regehr, W.G. (2020). Diverse roles of Synaptotagmin-7 in regulating vesicle fusion. Curr. Opin. Neurobiol. *63*, 42–52.

Iremonger, K.J., and Bains, J.S. (2007). Integration of Asynchronously Released Quanta Prolongs the Postsynaptic Spike Window. J. Neurosci. *27*, 6684–6691.

Jackman, S.L., and Regehr, W.G. (2017). The Mechanisms and Functions of Synaptic Facilitation. Neuron *94*, 447–464.

Jackman, S.L., Turecek, J., Belinsky, J.E., and Regehr, W.G. (2016). The calcium sensor synaptotagmin 7 is required for synaptic facilitation. Nature *529*, 88–91.

Jiang, M., Zhu, J., Liu, Y., Yang, M., Tian, C., Jiang, S., Wang, Y., Guo, H., Wang, K., and Shu, Y. (2012). Enhancement of asynchronous release from fast-spiking interneuron in human and rat epileptic neocortex. PLoS Biol. *10*.

Kaeser, P.S., and Regehr, W.G. (2014). Molecular mechanisms for synchronous, asynchronous, and spontaneous neurotransmitter release. Annu. Rev. Physiol. *76*, 333–363.

Khan, M.M., and Regehr, W.G. (2020). Loss of doc2b does not influence transmission at purkinje cell to deep nuclei synapses under physiological conditions. Elife *9*, 1–13.

Kusick, G.F., Chin, M., Raychaudhuri, S., Lippmann, K., Adula, K.P., Hujber, E.J., Vu, T., Davis, M.W., Jorgensen, E.M., and Watanabe, S. (2020). Synaptic vesicles transiently dock to refill release sites. Nat. Neurosci. *23*, 1329–1338.

Kusick, G.F., Ogunmowo, T.H., and Watanabe, S. (2022). Transient docking of synaptic vesicles: Implications and mechanisms. Curr. Opin. Neurobiol. *74*.

Li, S., Raychaudhuri, S., Lee, S.A., Brockmann, M.M., Wang, J., Kusick, G., Prater, C., Syed, S., Falahati, H., Ramos, R., et al. (2021). Asynchronous release sites align with NMDA receptors in mouse hippocampal synapses. Nat. Commun. *12*, 1–13.

Liu, H., Bai, H., Hui, E., Yang, L., Evans, C.S., Wang, Z., Kwon, S.E., and Chapman, E.R. (2014). Synaptotagmin 7 functions as a Ca2+-sensor for synaptic vesicle replenishment. Elife.

Manseau, F., Marinelli, S., Méndez, P., Schwaller, B., Prince, D.A., Huguenard, J.R., and Bacci, A. (2010). Desynchronization of neocortical networks by asynchronous release of GABA at autaptic and synaptic contacts from fast-spiking interneurons. PLoS Biol. *8*.

Marvin, J.S., Borghuis, B.G., Tian, L., Cichon, J., Harnett, M.T., Akerboom, J., Gordus, A., Renninger, S.L., Chen, T.W., Bargmann, C.I., et al. (2013). An optimized

fluorescent probe for visualizing glutamate neurotransmission. Nat. Methods *10*, 162–170.

Marvin, J.S., Scholl, B., Wilson, D.E., Podgorski, K., Kazemipour, A., Mueller, J.A., Schoch-McGovern, S., Wang, S.S.-H., Urra Quiroz, F.J., Rebola, N., et al. (2018). Stability, affinity and chromatic variants of the glutamate sensor iGluSnFR. Nat. Methods *15*.

Maximov, A., Lao, Y., Li, H., Chen, X., Rizo, J., Sorensen, J.B., and Sudhof, T.C. (2008). Genetic analysis of synaptotagmin-7 function in synaptic vesicle exocytosis. Proc Natl Acad Sci U S A *105*, 3986–3991.

Miki, T., Malagon, G., Pulido, C., Llano, I., Neher, E., and Marty, A. (2016). Actin- and Myosin-Dependent Vesicle Loading of Presynaptic Docking Sites Prior to Exocytosis. Neuron *91*, 808–823.

Miki, T., Nakamura, Y., Malagon, G., Neher, E., and Marty, A. (2018). Two-component latency distributions indicate two-step vesicular release at simple glutamatergic synapses. Nat. Commun.

Neher, E., and Brose, N. (2018). Dynamically Primed Synaptic Vesicle States: Key to Understand Synaptic Short-Term Plasticity. Neuron *100*, 1283–1291.

Otsu, Y., Shahrezaei, V., Li, B., Raymond, L.A., Delaney, K.R., and Murphy, T.H. (2004). Competition between Phasic and Asynchronous Release for Recovered Synaptic Vesicles at Developing Hippocampal Autaptic Synapses. J. Neurosci. *24*, 420–433.

Sabatini, B.L., and Regehr, W.G. (1996). Timing of neurotransmission at fast synapses in the mammalian brain. Nature *384*, 170–172.

Sakaguchi, G., Manabe, T., Kobayashi, K., Orita, S., Sasaki, T., Naito, A., Maeda, M., Igarashi, H., Katsuura, G., Nishioka, H., et al. (1999). Doc2α is an activity-dependent modulator of excitatory synaptic transmission. Eur. J. Neurosci. *11*, 4262–4268.

Silva, M., Tran, V., and Marty, A. (2021). Calcium-dependent docking of synaptic vesicles. Trends Neurosci. *44*, 579–592.

Stevens, C.F., and Sullivan, J.M. (2003). The synaptotagmin C2A domain is part of the calcium sensor controlling fast synaptic transmission. Neuron *39*, 299–308.

Truett, G.E., Heeger, P., Mynatt, R.L., Truett, A.A., Walker, J.A., and Warman, M.L. (2000). Preparation of PCR-quality mouse genomic dna with hot sodium hydroxide and tris (HotSHOT). Biotechniques *29*, 52–54.

Turecek, J., and Regehr, W.G. (2019). Neuronal Regulation of Fast Synaptotagmin Isoforms Controls the Relative Contributions of Synchronous and Asynchronous Release. Neuron *101*.

Turecek, J., and Regehr, X.W.G. (2018). Synaptotagmin 7 Mediates Both Facilitation and Asynchronous Release at Granule Cell Synapses. J. Neurosci. *38*, 3240–3251.

Vevea, J.D., and Chapman, E.R. (2020). Acute disruption of the synaptic vesicle membrane protein synaptotagmin 1 using knockoff in mouse hippocampal neurons. Elife *9*, 1–24.

Vevea, J.D., Kusick, G.F., Chen, E., Courtney, K.C., Watanabe, S., and Chapman, E.R. (2021). Synaptotagmin 7 is enriched at the plasma membrane through γ-secretase processing to promote vesicle docking and control synaptic plasticity in

mouse hippocampal neurons. Elife.

Watanabe, S., Davis, M.W., Kusick, G.F., Iwasa, J., and Jorgensen, E.M. (2020). SynapsEM: computer-assisted synapse morphometry. Front. Synaptic Neurosci.

Wen, H., Linhoff, M.W., Mcginley, M.J., Li, G., Corson, G.M., Mandel, G., and Brehm, P. (2010). Distinct roles for two synaptotagmin isoforms in synchronous and asynchronous transmitter release at zebra fish neuromuscular junction. Proc. Natl. Acad. Sci. *107*, 13906–13911.

Xue, R., Gaffaney, J.D., and Chapman, E.R. (2015). Structural elements that underlie Doc2β function during asynchronous synaptic transmission. Proc. Natl. Acad. Sci. *112*, E4316–E4325.

Xue, R., Ruhl, D.A., Briguglio, J.S., Figueroa, A.G., Pearce, R.A., and Chapman, E.R. (2018). Doc2-mediated superpriming supports synaptic augmentation. Proc. Natl. Acad. Sci. U. S. A. *115*, E5605–E5613.

Yao, J., Gaffaney, J.D., Kwon, S.E., and Chapman, E.R. (2011). Doc2 is a Ca 2+ sensor required for asynchronous neurotransmitter release. Cell *147*, 666–677.

Acknowledgments

We thank J.D. Vevea, M.M. Bradberry, K.C. Courtney, D. Larson, C. Greer, R.A. Pearce, and M. Seibert for help with iGluSnFR imaging, maintaining mouse strains, and data analysis and interpretation. We thank S. Myers for the improved fast DNA prep protocol. We thank all other members of the Chapman and Watanabe labs for helpful feedback and discussions. This work was funded by the National Institutes of Health (MH061876 and NS097362 to E.R.C.;1DP2 NS111133-01 and 1R01 NS105810-01A1 to S.W.), the National Science Foundation (1727260 to S.W.). E.R.C. is an Investigator of the Howard Hughes Medical Institute. S.W. is an Alfred P. Sloan fellow, a McKnight Foundation Scholar and a Klingenstein and Simons Foundation scholar. G.F.K. was supported by a grant from the National Institutes of Health to the Biochemistry, Cellular and Molecular Biology program of the Johns Hopkins University School of Medicine (T32 GM007445). G.F.K. was supported by a National Science Foundation Graduate Research Fellowship (2016217537) and is a Hay Fellow of the Johns Hopkins University School of Medicine Department of Cell Biology. The EM ICE high-pressure freezer was purchased partly with funds from an equipment grant from the National Institutes of Health (S10RR026445) awarded to S. C. Kuo.

Contributions

Z.W., G.F.K., E.R.C., and S.W. designed the study and wrote the manuscript. Z.W. performed all iGluSnFR and electrophysiology experiments, analyzed the corresponding data, and generated the corresponding figures. G.F.K. performed all electron microscopy experiments, with help from S.R, analyzed the corresponding data with S.W., and generated the corresponding figures with S.W. K.I., S.R., and G.F.K. performed knockout cell culture for the electron microscopy experiments. E.R.C. and S.W. funded and oversaw the research.

Ethics declarations

Competing interests

The authors declare no competing interests.

Figure 1

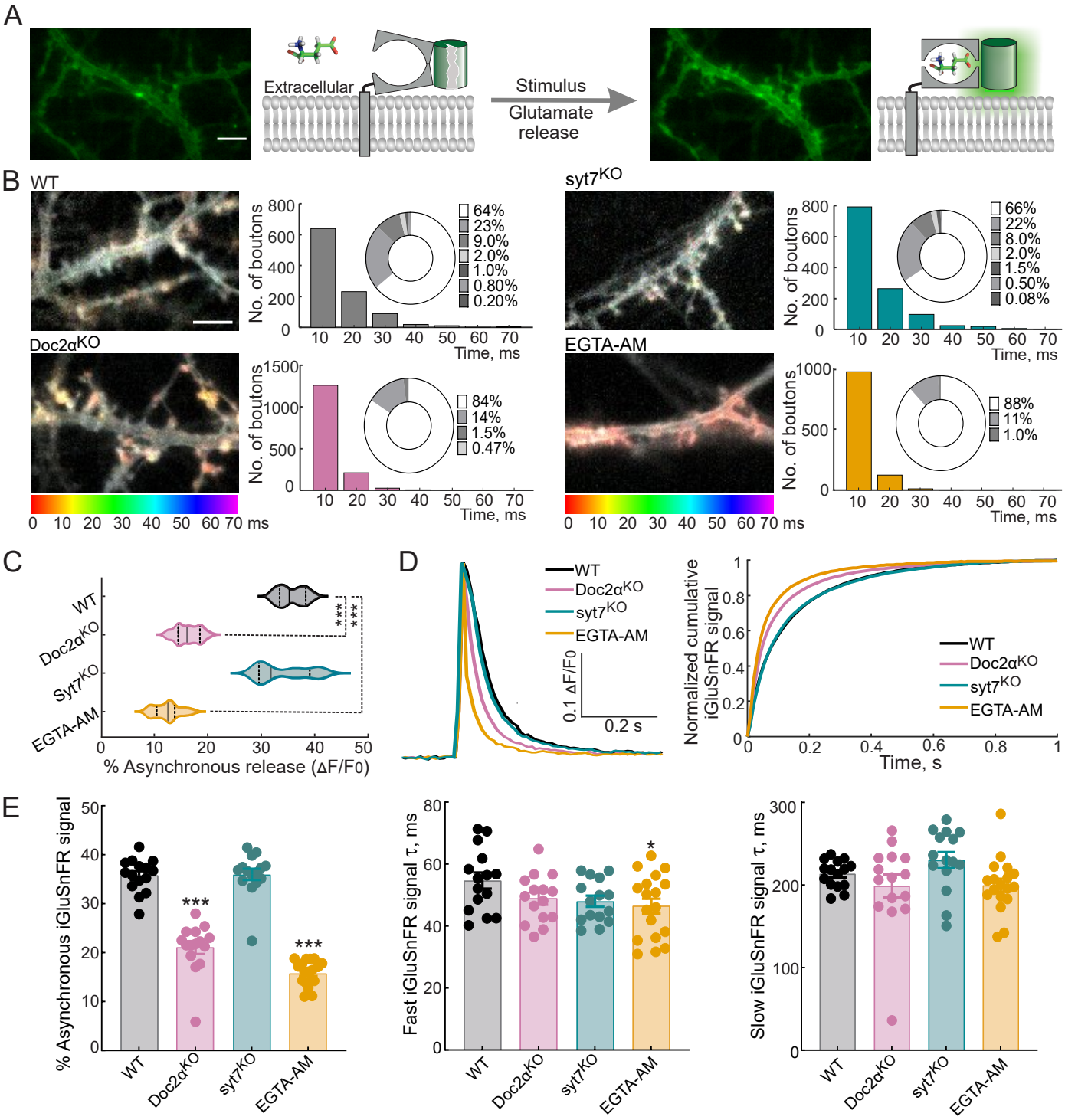
A
Extracellular
Stimulus
Glutamate release
B
WT
No. of boutons
Time, ms
64%
23%
9.0%
2.0%
1.0%
0.80%
0.20%
syt7KO
66%
22%
8.0%
2.0%
1.5%
0.50%
0.08%
Doc2αKO
84%
14%
1.5%
0.47%
EGTA-AM
88%
11%
1.0%
0 10 20 30 40 50 60 70 ms
C
WT
Doc2αKO
Syt7KO
EGTA-AM
% Asynchronous release (ΔF/F0)
D
WT
Doc2αKO
syt7KO
EGTA-AM
0.1 ΔF/F0
0.2 s
Normalized cumulative iGluSnFR signal
Time, s
E
% Asynchronous iGluSnFR signal
Fast iGluSnFR signal τ, ms
Slow iGluSnFR signal τ, ms

Figure 2

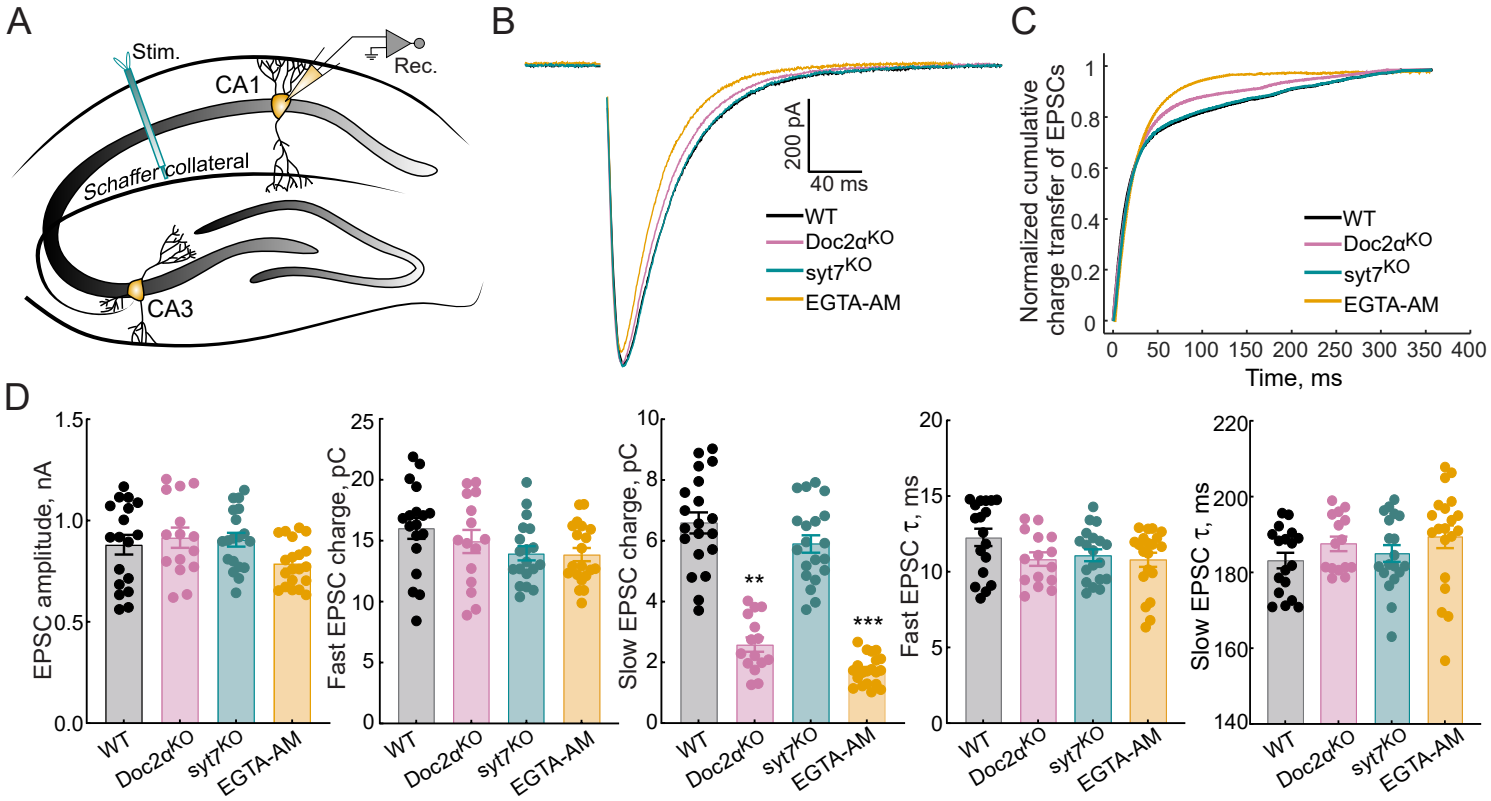
A
Stim.
Rec.
CA1
Schaffer collateral
CA3
B
200 pA
40 ms
WT
Doc2αKO
syt7KO
EGTA-AM
C
Normalized cumulative charge transfer of EPSCs
Time, ms
D
EPSC amplitude, nA
Fast EPSC charge, pC
Slow EPSC charge, pC
Fast EPSC τ, ms
Slow EPSC τ, ms
**
***
WT
Doc2αKO
syt7KO
EGTA-AM

Figure 3

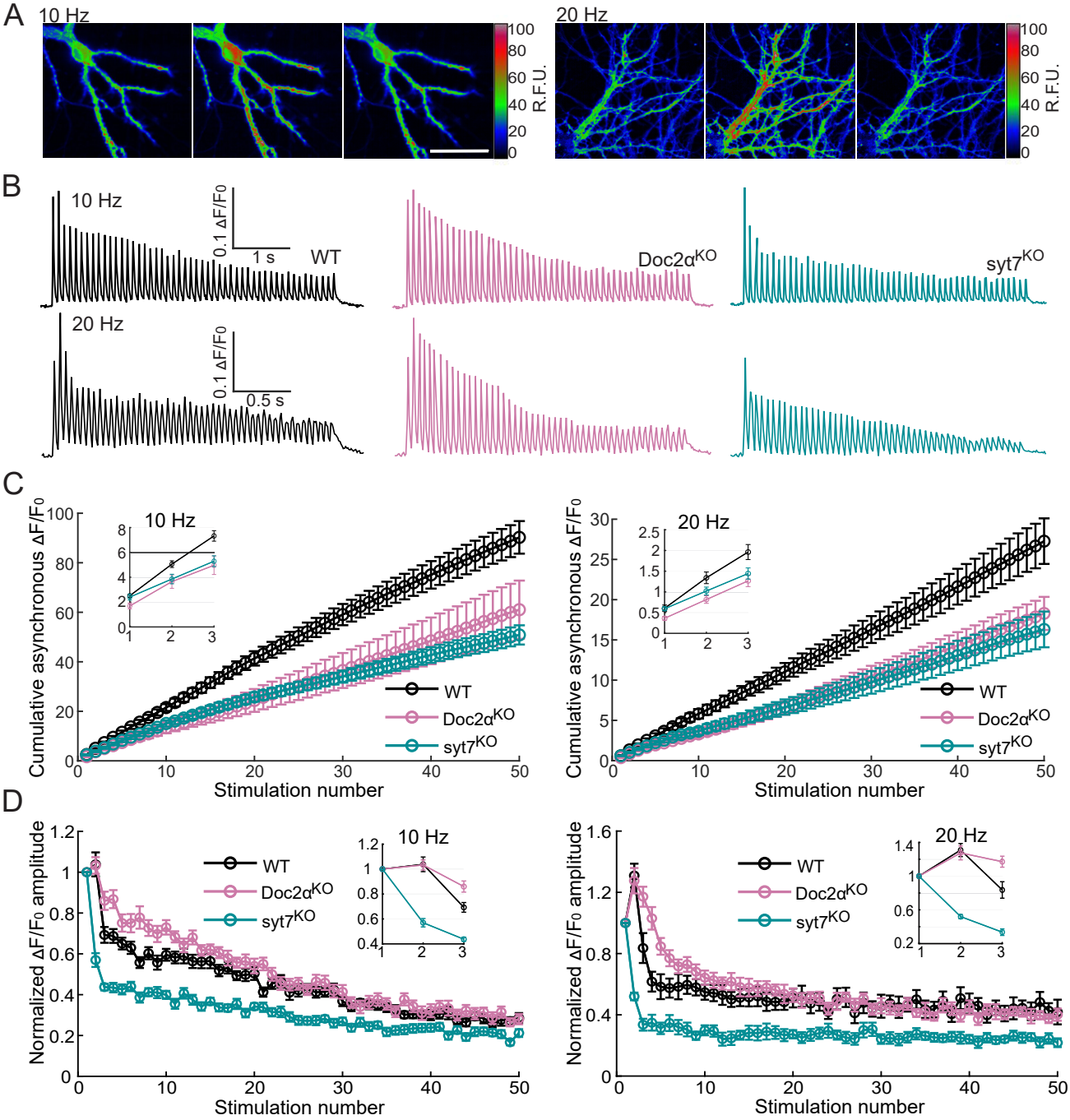
A
10 Hz
20 Hz
R.F.U.
B
10 Hz
0.1 ΔF/F0
1 s
WT
Doc2α^KO
syt7^KO
20 Hz
0.5 s
C
Cumulative asynchronous ΔF/F0
Stimulation number
WT
Doc2α^KO
syt7^KO
D
Normalized ΔF/F0 amplitude

Figure 4

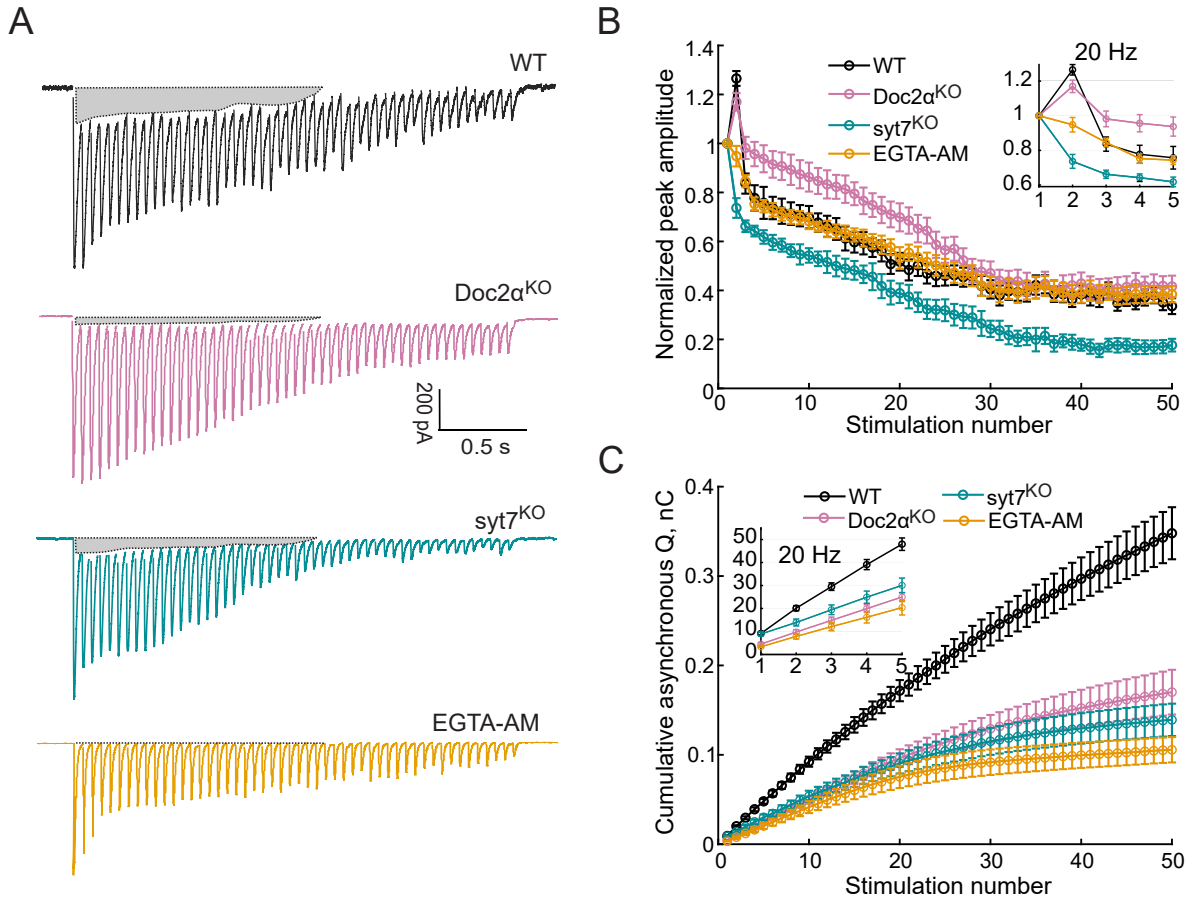
A
WT
Doc2α^{KO}
200 pA
0.5 s
syt7^{KO}
EGTA-AM
B
Normalized peak amplitude
Stimulation number
WT
Doc2α^{KO}
syt7^{KO}
EGTA-AM
20 Hz
C
Cumulative asynchronous Q, nC
Stimulation number
WT
Doc2α^{KO}
syt7^{KO}
EGTA-AM
20 Hz

Figure 5

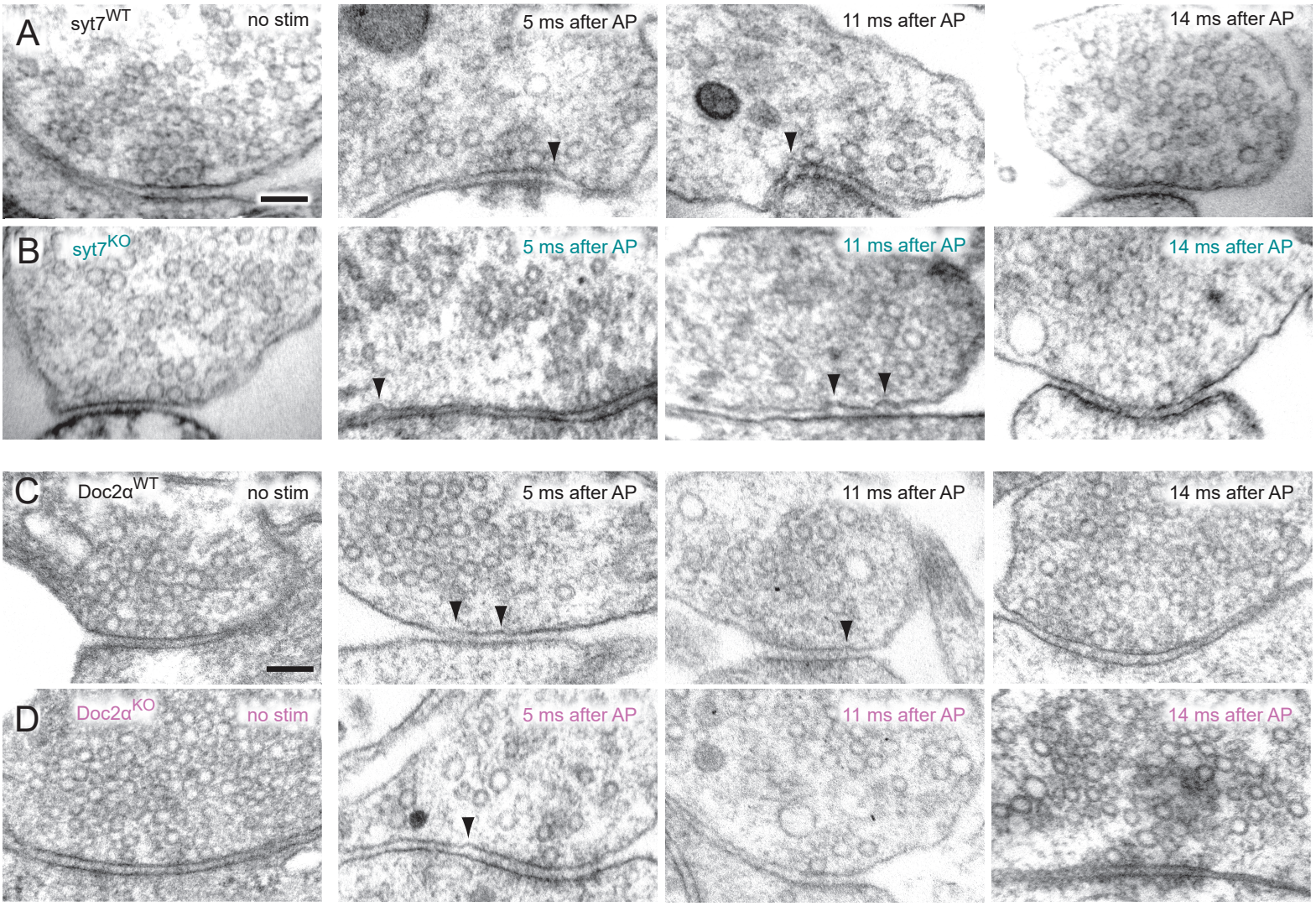
A
syt7WT
no stim
5 ms after AP
11 ms after AP
14 ms after AP
B
syt7KO
5 ms after AP
11 ms after AP
14 ms after AP
C
Doc2αWT
no stim
5 ms after AP
11 ms after AP
14 ms after AP
D
Doc2αKO
no stim
5 ms after AP
11 ms after AP
14 ms after AP

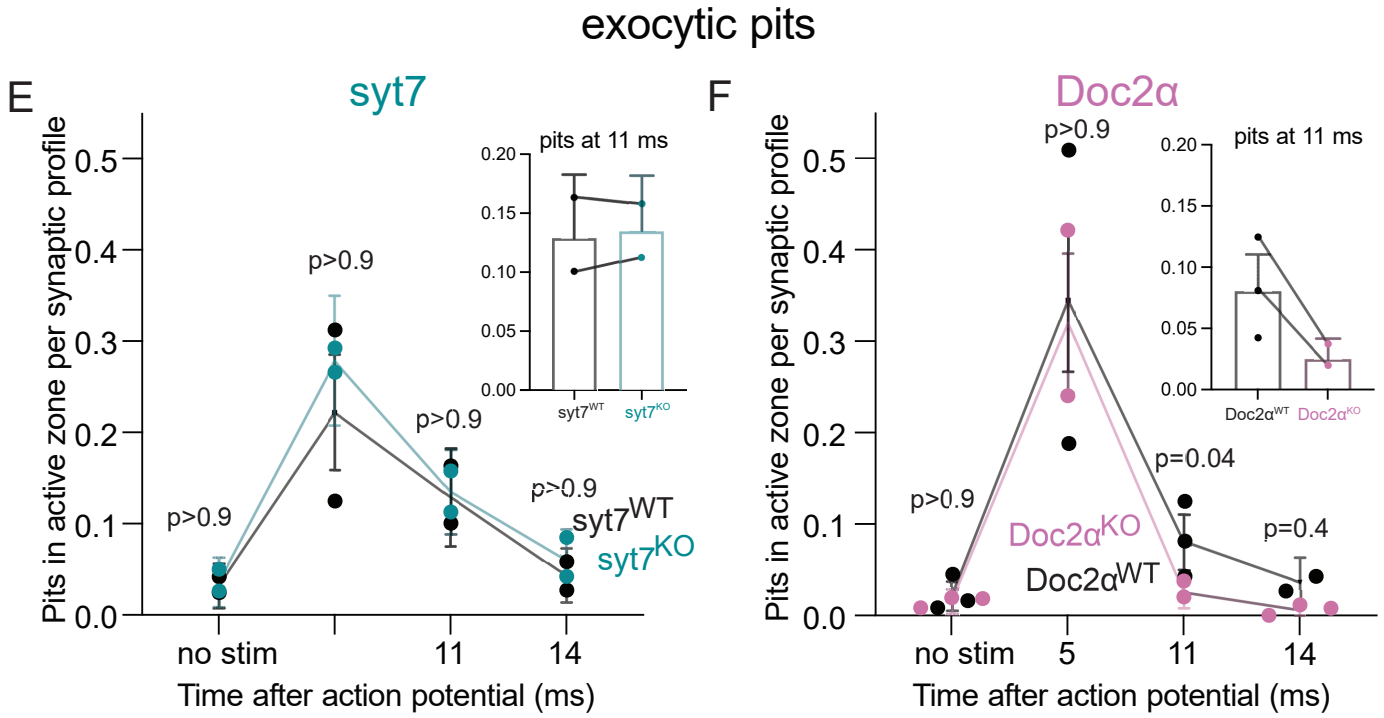
exocytic pits
E
syt7
Pits in active zone per synaptic profile
0.0
0.1
0.2
0.3
0.4
0.5
p>0.9
p>0.9
p>0.9
p>0.9
syt7WT
syt7KO
no stim
11
14
Time after action potential (ms)
pits at 11 ms
0.00
0.05
0.10
0.15
0.20
syt7WT
syt7KO
F
Doc2α
Pits in active zone per synaptic profile
p>0.9
p>0.9
p=0.04
p=0.4
Doc2αKO
Doc2αWT
no stim
5
11
14
Time after action potential (ms)
pits at 11 ms
Doc2αWT
Doc2αKO

Figure 6

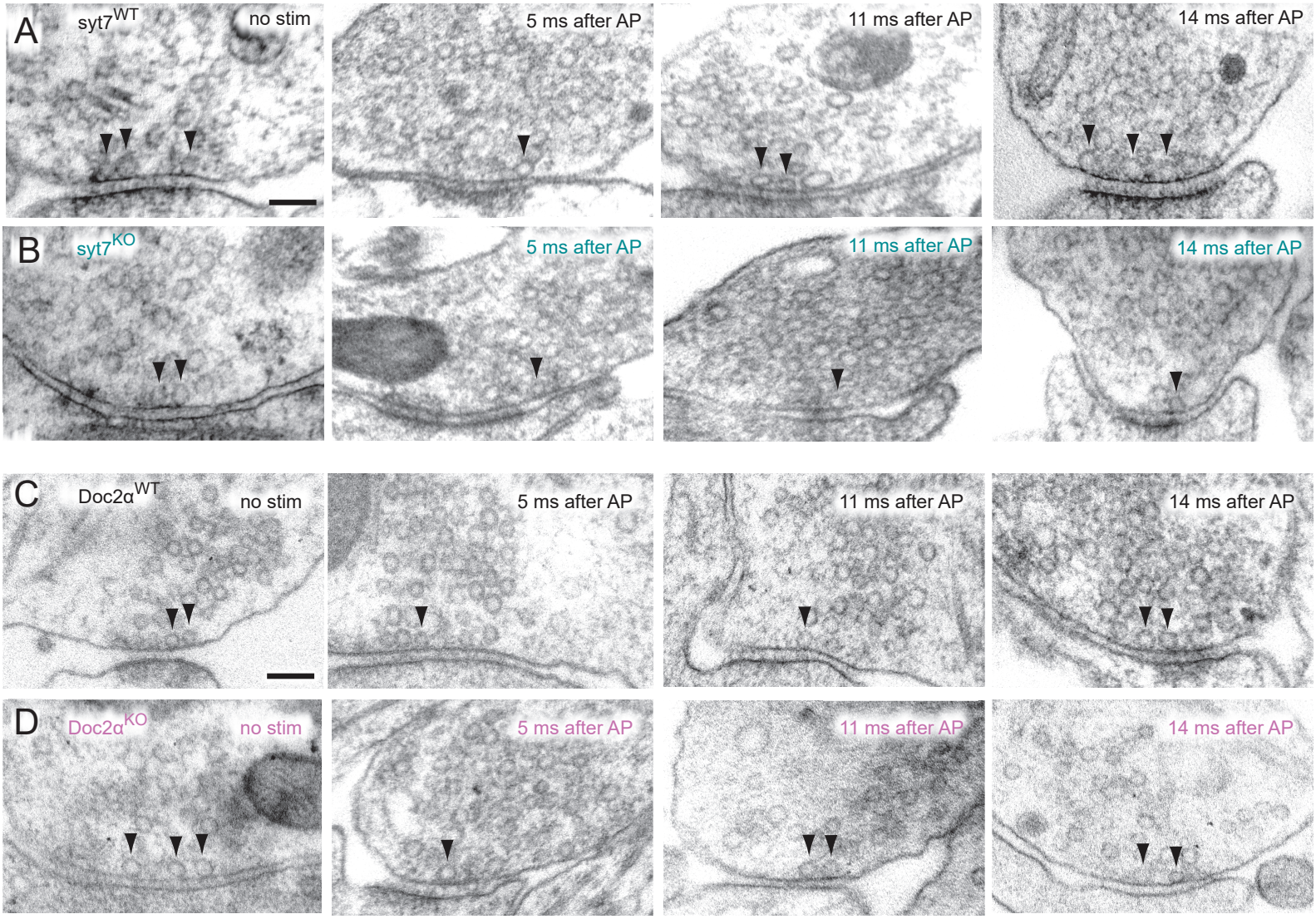
A
syt7WT
no stim
5 ms after AP
11 ms after AP
14 ms after AP
B
syt7KO
5 ms after AP
11 ms after AP
14 ms after AP
C
Doc2αWT
no stim
5 ms after AP
11 ms after AP
14 ms after AP
D
Doc2αKO
no stim
5 ms after AP
11 ms after AP
14 ms after AP

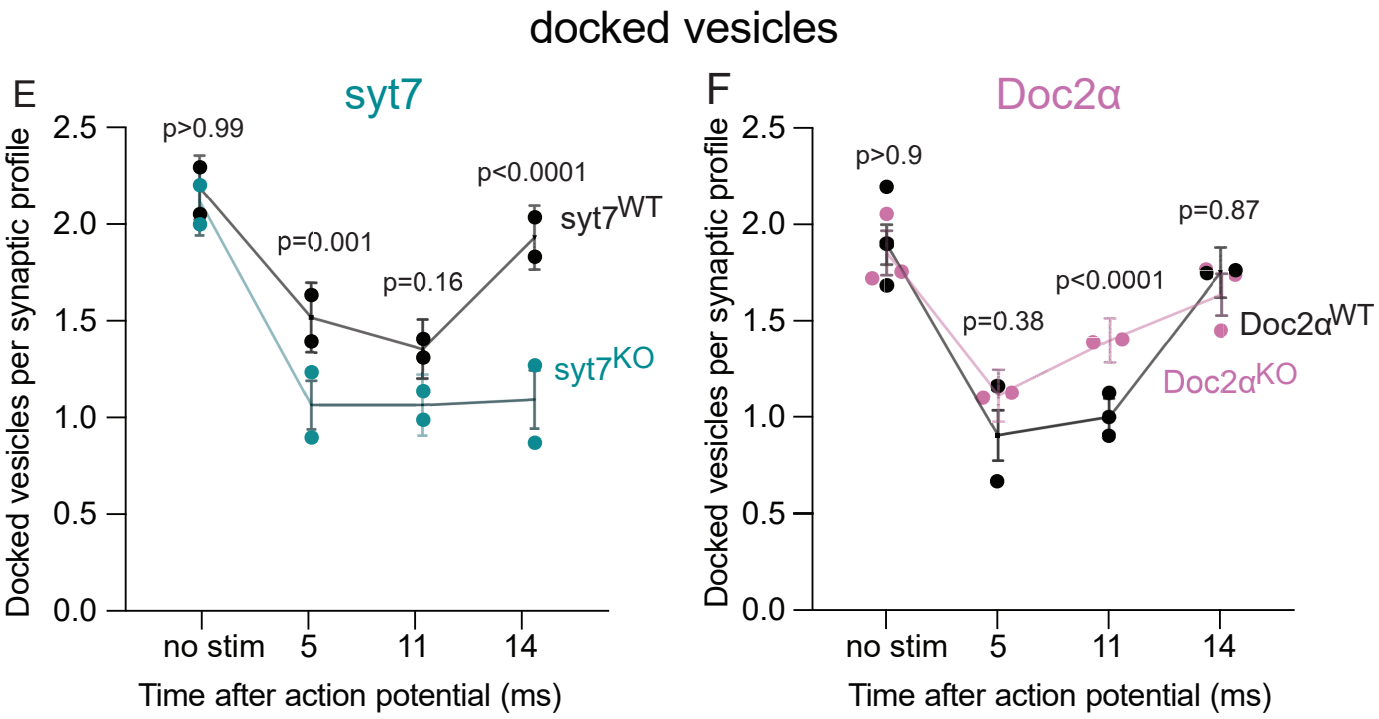
docked vesicles
E
syt7
Docked vesicles per synaptic profile
2.5
2.0
1.5
1.0
0.5
0.0
p>0.99
p=0.001
p=0.16
p<0.0001
syt7WT
syt7KO
no stim
5
11
14
Time after action potential (ms)
F
Doc2α
Docked vesicles per synaptic profile
2.5
2.0
1.5
1.0
0.5
0.0
p>0.9
p=0.38
p<0.0001
p=0.87
Doc2αWT
Doc2αKO
no stim
5
11
14
Time after action potential (ms)

Figure 7

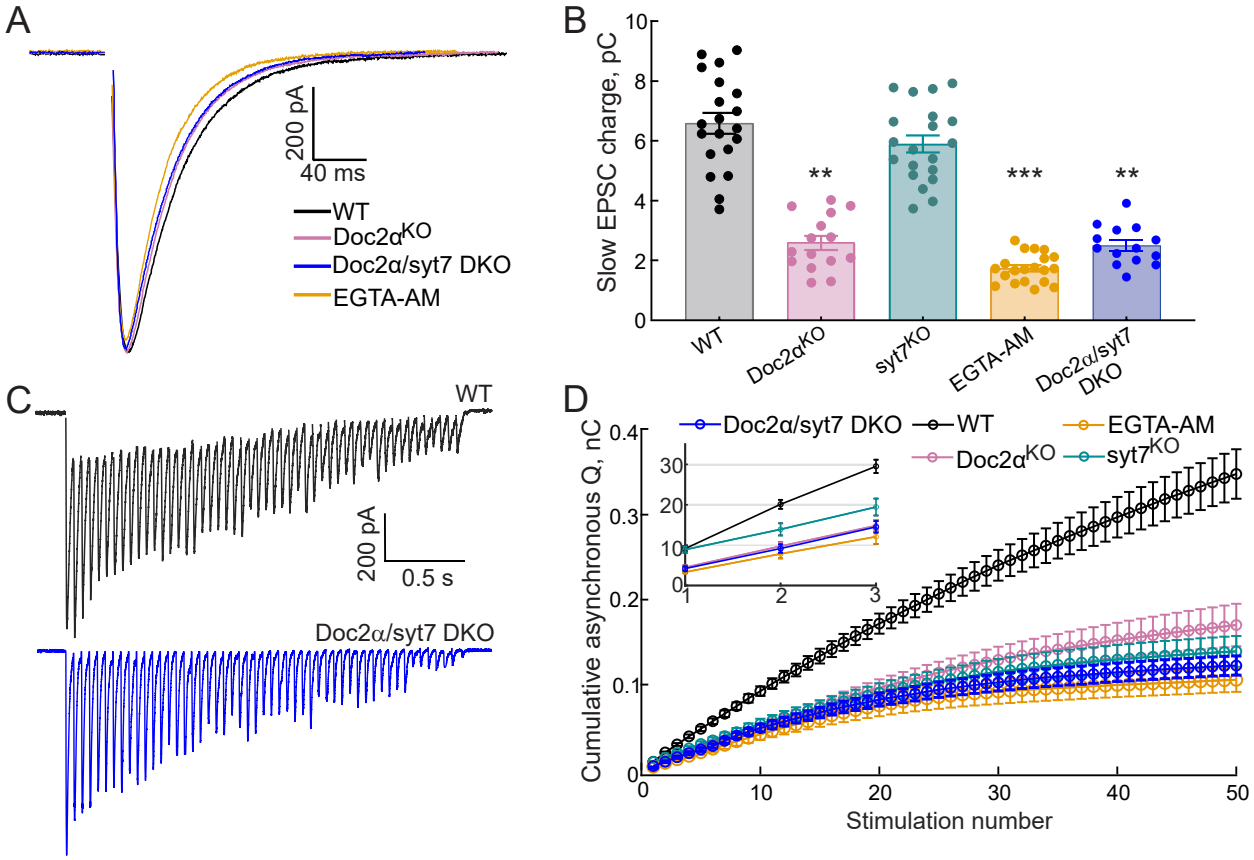
A
200 pA
40 ms
WT
Doc2α^KO
Doc2α/syt7 DKO
EGTA-AM
B
Slow EPSC charge, pC
10
8
6
4
2
0
**
***
**
WT
Doc2α^KO
syt7^KO
EGTA-AM
Doc2α/syt7 DKO
C
WT
200 pA
0.5 s
Doc2α/syt7 DKO
D
Doc2α/syt7 DKO
WT
EGTA-AM
Doc2α^KO
syt7^KO
Cumulative asynchronous Q, nC
0.4
0.3
0.2
0.1
0
30
20
10
0
1
2
3
0
10
20
30
40
50
Stimulation number